resistance to neutralization (**Figure 3A**). Recombinants SN and NS, which have substitutions in gp120 and gp41 from P26B404I, respectively, showed varying degrees of resistance. The IC_{50} values of SN and NS against B404 were intermediates between the parental SIVmac316 and the neutralization-resistant P26B404. Maximal inhibition reached a plateau at 73.8, 82.3, and 81.9% in SS, NS, and P26B404, respectively, but the MPI value of SN (94.9%) was close to that of SIVmac316 (100%; **Figure 3B**). Neutralization resistance to anti-CD4i MAb K8 was characterized by decreases in the IC_{50} value of SN and the MPI of NS. Neutralization by anti-V2 MAb M318T was even enhanced in SN, although NS showed the resistance comparable to those of SS and P26B404. The decreases in MPI values were commonly observed for the neutralization of NS by the three MAbs (**Figure 3B**). Resistance to neutralization was not significantly detected by the point mutants F277V and N295S, except for the neutralization of F277V by K8 (4.3-fold decrease of IC_{50} value). These results indicated that the entire *env* region, including substitutions in both gp120 and gp41, was responsible for the full-resistance of P26B404 to neutralization. The decrease of MPI values for NS suggested that truncation of gp41 by the Q733stop substitution, the first major substitution in viral evolution, was important to escape from the neutralizing antibodies.

INCREASED INFECTIVITY FOR HUMAN CELLS BY SIV WITH A TRUNCATED gp41

Truncation of gp41 in SIV is associated with the adaptation to human cells (Hirsch et al., 1989; Kodama et al., 1989), which may partially contribute to neutralization resistance (Yuste et al., 2005). To explore the mechanism of neutralization resistance of P26B404, the infectivity of recombinant viruses was analyzed by determining the $TCID_{50}$ values of virus stocks prepared by transfection of 293T cells (**Table 2**). The $TCID_{50}$ values in all the human cells tested were significantly higher for SS and NS viruses with truncated gp41 than

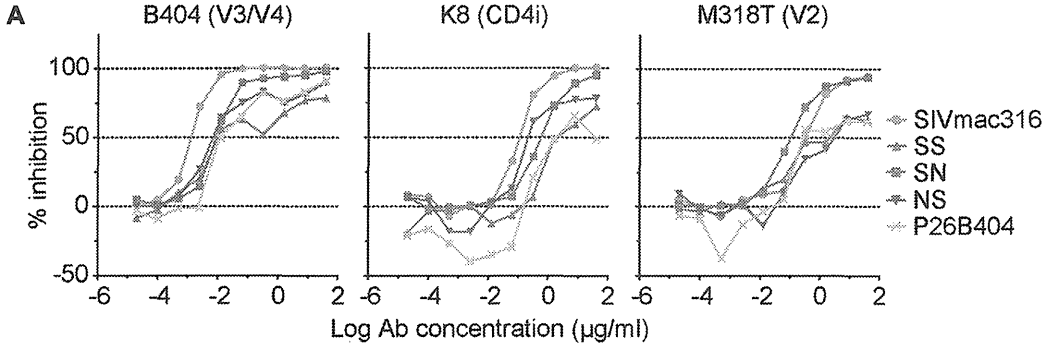

B

Neutralization profile of mutant viruses

Virus	B404 (V3/V4)		K8 (CD4i)		M318T (V2)	
	IC_{50}	MPI	IC_{50}	MPI	IC_{50}	MPI
SIVmac316	1.3E-03 (1.0)	100 (0.0)	1.1E-01 (1.0)	99.0 (0.0)	3.3E-01 (1.0)	94.3 (0.0)
SS	1.9E-02 (14.5)	73.8 (-26.2)	1.8E+00 (16.3)	67.9 (-31.1)	9.4E-01 (2.8)	65.5 (-28.8)
SN	9.1E-03 (6.8)	94.9 (-5.1)	5.9E-01 (5.3)	94.7 (-4.4)	1.0E-01 (0.3)	92.5 (-1.8)
NS	6.8E-03 (5.1)	82.3 (-17.7)	2.1E-01 (1.9)	77.0 (-22.0)	1.7E+00 (5.2)	67.6 (-26.7)
F277V	3.8E-03 (2.8)	100 (0.0)	4.8E-01 (4.3)	99.6 (0.5)	3.0E-01 (0.9)	94.8 (0.5)
N295S	2.3E-03 (1.7)	99.6 (-0.4)	1.4E-01 (1.2)	99.9 (0.8)	3.1E-01 (0.9)	97.0 (2.7)
P26B404	1.7E-02 (12.5)	81.9 (-18.1)	8.2E-01 (7.3)	54.6 (-44.5)	2.5E-01 (0.8)	60.0 (-34.3)

Fold change of IC_{50}	% change of MPI
> 10	< -20
3-10	-10- to -20
< 3	> -10

FIGURE 3 | Sensitivities of viruses with B404-resistant mutations to neutralization by MAbs. (A) Sensitivities of mutant viruses SS, SN, and NS to neutralization by MAbs Fab-B404 (anti-V3/V4), Fab-K8 (anti-CD4i), and M318T (anti-V2) are shown. Neutralization of parental SIVmac316 and B404-resistant P26B404 is also shown as controls sensitive and resistant to neutralization, respectively. **(B)** The sensitivities to neutralization are represented by values for IC_{50} (μg/ml) and MPI (%). Viruses were examined for their sensitivities to neutralization by MAbs Fab-B404, Fab-K8, and M318T in TZM-bl cells. The IC_{50} and MPI values were determined using Prism 5. The fold-change of IC_{50} was calculated by dividing the IC_{50} value by that of the parental SIVmac316. Percent change of MPI was calculated by subtracting the MPI value from that of SIVmac316. These changes are shown in parentheses and significant changes are indicated by magenta (IC_{50}: >10; MPI: < −20) and orange (IC_{50}: 3–10; MPI: −20 to −10) highlighting.

parental SIVmac316 and SN, in which gp41 is intact. In particular, NS showed a striking increase in $TCID_{50}$ values, which were 7,100-, 1,000-, and 140-fold higher than those of parental SIVmac316 in PM1, PM1/CCR5, and TZM-bl cells, respectively. These results indicate that truncation of gp41 caused by the Q733stop substitution increases viral infectivity for human cells.

To compare viral infectivity in human and macaque cells, viral infection was monitored after inoculation of PM1 and PM1/CCR5 human cells and the HSC-F cynomolgus macaque cell line with varying dilutions of virus stocks (**Figure 4**). Consistent with the $TCID_{50}$ analysis, a higher frequency of infected cells was detected earlier in PM1 and PM1/CCR5 cells inoculated with NS than the parental SIVmac316. In contrast, SN showed decreased infectivity in PM1 and PM1/CCR5 cells, apparently because PM1 cells were not infected by a 1,000-fold diluted SN stock. Although the $TCID_{50}$ values of SS were much higher than those of SIVmac316, the replication kinetics of SS were similar to those of SIVmac316 in PM1 and PM1/CCR5 cells. These results suggest that gp41 truncation increases infectivity for human cells and that the substitutions in gp120 of P26B404I are associated with slow and poor replication compared with that of SIVmac316.

Infectivity for macaque cells was more significantly affected than that for human cells by the substitutions in gp120 of P26B404I (**Figure 4**, lower panels). Infected cells were detected in HSC-F cells inoculated with 1,000-fold diluted virus stocks of SIVmac316 and NS, but viral infection in HSC-F cells was limited to a low frequency even by inoculation with 10-fold diluted virus stocks of SS and SN. Truncation of gp41 did not significantly affect replication in HSC-F macaque cells, although truncation of gp41 was disadvantageous for replication in primary T cell cultures from macaques (Hirsch et al., 1989; Kodama et al., 1989).

These results demonstrate that gp41 truncation strikingly increases infectivity for human cells, but not for macaque cells, and that the substitutions in gp120 decrease infectivity in human and macaque cells. Truncation of gp41, which conferred extremely high infectivity for PM1/CCR5 cells, may be the first step to escape from neutralization and the substitutions in gp120 may be the second step to replicate in the presence of high concentration of B404.

Table 2 | Infectivity* of viruses with substitutions from P26B404.

Viruses	PM1	PM1/CCR5	TZM-bl
SIVmac316	4.2E+02 (1.0)	1.4E+03 (1.0)	9.6E+04 (1.0)
SS	2.9E+05 (710)	4.7E+05 (350)	6.3E+06 (66)
SN	2.0E+03 (4.8)	8.4E+03 (6.2)	2.9E+05 (3.1)
NS	2.9E+06 (7,100)	1.4E+06 (1,000)	1.4E+07 (140)

**Infectivity is shown by the $TCID_{50}$/ml values of the viruses, which were prepared by transfection of 293T cells, in PM1, PM1/CCR5, and TZM-bl cells. The fold-change, which was calculated by dividing the mutant $TCID_{50}$/ml value by that of the parental SIVmac316, is shown in the parentheses.*

INCREASED INCORPORATION OF Env INTO VIRIONS IN SIV WITH TRUNCATED gp41

Incorporation of Env into virions was examined using these recombinant viruses, because increased infectivity by gp41 truncation was suggested to be associated with the Env content of virions (Manrique et al., 2001; Zhu et al., 2003, 2006; Yuste et al., 2004, 2005). Analysis of viral proteins in cells and supernatants from transfected 293T cells revealed that incorporation of Env into virions was significantly high in SS and NS viruses with the Q733stop substitution (**Figure 5**). MAb to gp120 showed a higher amount

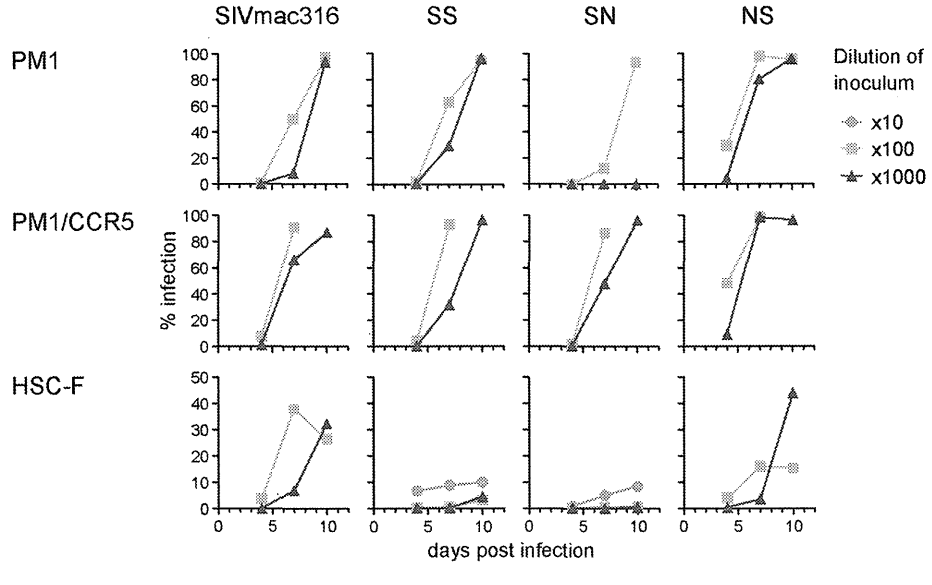

FIGURE 4 | Replication of B404-resistant viruses in human and macaque cells. Frequencies of infected cells at 4, 7, and 10 days post-infection are shown. PM1 and PM1/CCR5 human T cells and HSC-F cynomolgus macaque T cells were infected with the various dilutions of SIVmac316, SS, SN, and NS. Infected cells were detected using flow cytometry after intracellular staining by B450 (anti-p27 Fab).

of gp120 and gp160 in virions from SS and NS than those from SN and the parental SIVmac316, although the production of Env proteins in the transfected cells was at the same level among all the viruses (**Figure 5A**). MAb to gp41 also demonstrated that truncated gp41 was more abundant in virions compared with full-length gp41 (**Figure 5B**). Semi-quantification by densitometric scanning of gp41 and p26 images suggested that the levels of gp41 amount per virion in SS and NS were 12- and 44-fold higher than that of SIVmac316, respectively, after adjusting virion numbers using the p26 amounts. In contrast to the increased amount of Env proteins in virions from viruses with truncated gp41, the level of Gag p27 in virions was low in SS and NS compared with those in SN and SIVmac316 (**Figure 5C**). This indicates that the Env content per virion, which was normalized by the amount of p27, was significantly high in viruses with truncated gp41. These results suggest that truncation of gp41 by the Q733stop substitution enhances incorporation of Env into virions.

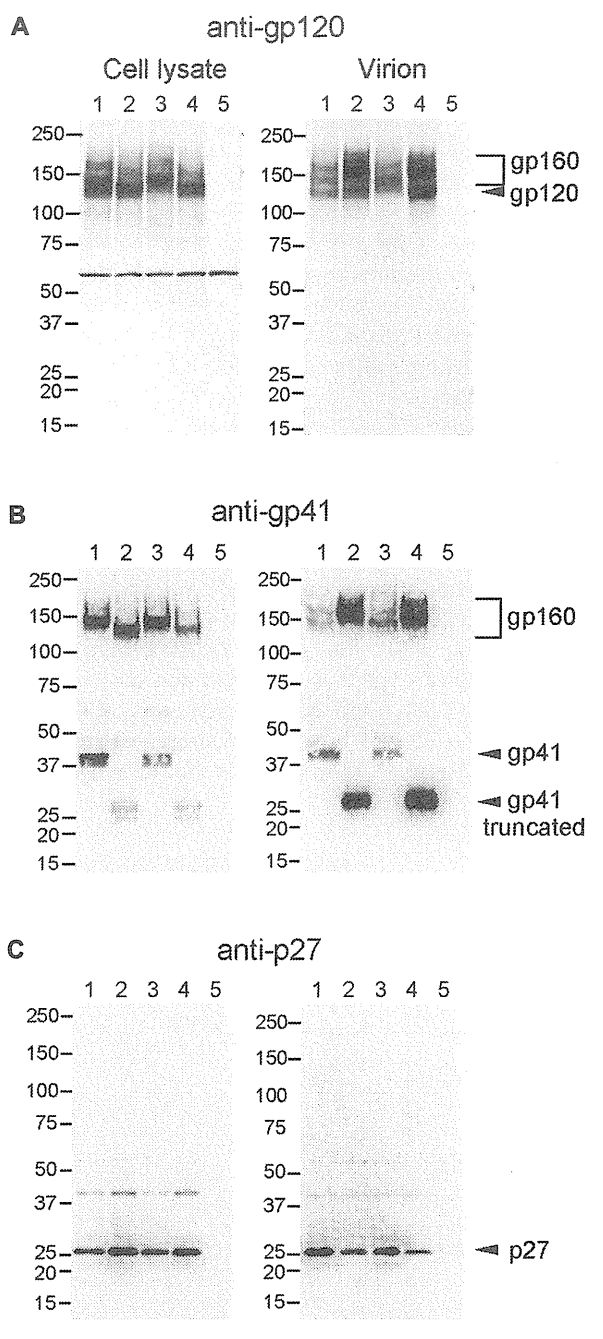

FIGURE 5 | Effect of B404-resistant mutations on the incorporation of Env into virions. Cell lysates (left panels) and virions (right panels) of SIVmac316 (lane 1), SS (lane 2), SN (lane 3), NS (lane 4), and mock-infected control (lane 5), which were prepared from transfected 293T cells, were analyzed by Western blotting. Viral proteins gp120 **(A)**, gp41 **(B)**, and p27 **(C)** were detected using MAbs M318T (anti-gp120 V2), B408 (anti-gp41 cluster I), and B450 (anti-p27), respectively.

NEUTRALIZATION RESISTANCE OF SIV WITH TRUNCATED gp41 IN MACAQUE CELLS

The analysis of infectivity of recombinant viruses suggested that the resistance to neutralization by truncation of gp41 might be due to adaptation to human cells. To examine this hypothesis, sensitivity to neutralization by B404 was determined in HSC-F macaque cells using SIVmac316 and NS, which showed similar infectivity for HSC-F cells (**Figure 4**). In flow cytometric analysis, infection in the presence or absence of B404 demonstrated that the high sensitivity of SIVmac316 and resistance of NS to neutralization were maintained in HSC-F cells (**Figure 6**). The frequency of infected cells decreased from 41.5% to the background level (2.03%) in inoculation with the undiluted stock of SIVmac316. In contrast, infection with NS, even with a 10-fold diluted virus stock, was significant in HSC-F cells in the presence of B404 (**Figure 6A**). Neutralization of NS in HSC-F cells was characterized by a decrease in maximal inhibition (**Figure 6B**), which was also observed in TZM-bl cells (**Figure 3A**). The magnitude of resistance of NS to B404 was greater when infection was performed using the undiluted stock compared with the 10-fold diluted stock, raising the possibility that B404 did not inhibit infection with a high titer of viruses. However, the resistance of NS was shown by infection with a low titer of NS, in which the frequency of infected cells in the absence of B404 (23.8%) was lower than infection with undiluted SIVmac316 (41.5%). Further, immunoblotting analysis revealed that the amount of virions was higher in the virus stock of SIVmac316 than that of NS (**Figure 5**).

These results indicate that gp41 truncation by the Q733stop substitution contributes to neutralization resistance of viruses in macaque cells. This suggests that the resistance to neutralization by truncation of gp41 is not due to the adaptation to human cells. The Q733stop substitution, the first major mutation during passages in the presence of B404, might be selected because it facilitates adaptation of virus to human cells and imparts resistance to antibody.

DISCUSSION

In the present study, truncation of the cytoplasmic tail of gp41, which was caused by the Q733stop substitution in Env, was the first major mutation detected during passage of SIV in the presence of the neutralizing antibody B404. Analysis of recombinant viruses suggested that the gp41 truncation was selected by their resistance to neutralizing antibody, which was characterized by the decrease of maximal inhibition compared with viruses with intact gp41, and

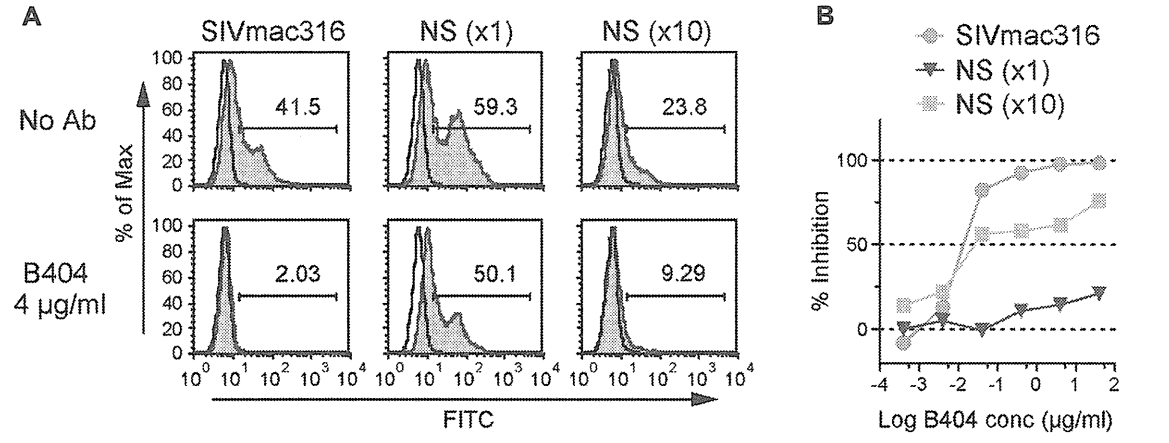

FIGURE 6 | Contribution of gp41 truncation to neutralization resistance in infection of macaque cells. (A) Infection of HSC-F cells in the presence (4 μg/ml) or absence of Fab-B404 is shown. HSC-F cells were inoculated with undiluted SIVmac316 and NS, and 10-fold diluted NS. Viral infection was monitored 4 days post-infection using flow cytometry after intracellular staining by B450 (anti-p27 Fab). **(B)** Neutralization of SIVmac316 and NS by B404 in HSC-F cells are shown. Percent inhibition was calculated by comparison with the infected culture in the absence of B404.

increased infectivity for human cells. The premature stop codon in the gp41 cytoplasmic region was frequently detected in SIV strains propagated in human cell culture *in vitro*, such as the original SIVmac316 clone, SIVmac1A11 and 17E-Fr (Hirsch et al., 1989; Kodama et al., 1989; Mori et al., 1992; Bonavia et al., 2005; Vzorov et al., 2005). The truncation of gp41 is considered as an adaptation of SIV to replication in human cell culture, because the premature stop codon rapidly reverted to express full-length gp41 after infection of rhesus primary cell culture *in vitro* and rhesus macaques *in vivo* (Hirsch et al., 1989; Kodama et al., 1989). Mutant viruses harboring the gp41 truncation showed increased infectivity for human cells, although the effects on infectivity varied depending on the SIV strain and the length of the gp41 truncation (Manrique et al., 2001; Yuste et al., 2004, 2005; Vzorov et al., 2005, 2007). The enhancement effect of gp41 truncation on incorporation of Env into virions, which were demonstrated by quantification of viral proteins in virions (Yuste et al., 2004) and electron tomography analysis of Env trimers on virions (Zhu et al., 2003, 2006), was partly associated with the increased infectivity caused by gp41 truncation (Manrique et al., 2001; Yuste et al., 2004, 2005). Because expression of Env on the cell surface is regulated by the cytoplasmic domain of gp41, truncation of gp41 may increase Env density on both cells and virions (LaBranche et al., 1995; Berlioz-Torrent et al., 1999; Postler and Desrosiers, 2013). Consistent with these studies, infectivity for human cells and Env incorporation into virions was enhanced by gp41 truncation in the present study. Although the mechanism responsible for increasing viral infectivity caused by gp41 truncation remains unclear, the high virion Env content may contribute to the efficient replication of viruses with truncated gp41 in human cells.

The effect of gp41 truncation on susceptibility to antibody-mediated neutralization is controversial, perhaps due to the SIV strains used for the analyses. Because most of prototypic SIV clones with truncated gp41 were macrophage-tropic, CD4-independent, and neutralization-sensitive (Mori et al., 1992; Bonavia et al., 2005; Vzorov et al., 2005), the truncation of gp41 was assumed responsible for the high sensitivity to neutralization. However, the resistance to neutralization by gp41 truncation was shown using the E767stop mutant of SIVmac316 (Yuste et al., 2005). This is consistent with our results using SIVmac316 harboring the Q733stop substitution, indicating that gp41 truncation contributes to resistance of SIVmac316 to neutralization. The increased infectivity of viruses with gp41 truncation in human cells may partially play a role in resistance by overcoming antibody-mediated neutralization via efficient attachment and entry of viruses to cells. However, we showed that gp41 truncation was also associated with neutralization resistance in macaque cells, in which gp41 truncation did not significantly affect infectivity. This suggests that the increased infectivity in human cells does not significantly affect the neutralization resistance of viruses with truncated gp41. As shown by provision of excess Env in trans, high Env content in virions may be critical for antibody-mediated neutralization (Yuste et al., 2005). Further studies will be required to understand the mechanism of resistance to neutralization conferred by gp41 truncation.

In the present study, we demonstrated that truncation of the cytoplasmic tail of gp41 contributes to resistance to antibody-mediated neutralization. Although non-human primate models of SIV infection are commonly used to estimate vaccine efficacy, the lack of broadly neutralizing MAbs has hampered development of antibody-based vaccine candidates in an SIV-macaque model. The broadly neutralizing MAb B404, which neutralizes multiple, diverse SIV isolates (Kuwata et al., 2013), is a useful tool for understanding the mechanism of neutralization in an SIV-macaque model and will contribute to the development of HIV-1 vaccines.

ACKNOWLEDGMENTS

We thank Dr. Hirofumi Akari for providing HSC-F cells. TZM-bl cells were obtained from Dr. John C. Kappes, Dr. Xiaoyun Wu, and Tranzyme Inc. through the NIH AIDS Research and Reference Reagent Program, Division of AIDS, NIAID, NIH. This work

was supported by MEXT KAKENHI Grant Number 10839786, the Program of Founding Research Centres for Emerging and Re-emerging Infectious Diseases, the Global COE program Global Education and Research Centre Aiming at the Control of AIDS and a grant-in-aid for scientific research (C-24591484) from the Ministry of Education, Culture, Sport, Science and Technology, Japan and a grant from the Ministry of Health, Welfare and Labour of Japan (H24-AIDS-007).

REFERENCES

Akari, H., Nam, K. H., Mori, K., Otani, I., Shibata, H., Adachi, A., et al. (1999). Effects of SIVmac infection on peripheral blood CD4+CD8+ T lymphocytes in cynomolgus macaques. *Clin. Immunol.* 91, 321–329.

Berlioz-Torrent, C., Shacklett, B. L., Erdtmann, L., Delamarre, L., Bouchaert, I., Sonigo, P., et al. (1999). Interactions of the cytoplasmic domains of human and simian retroviral transmembrane proteins with components of the clathrin adaptor complexes modulate intracellular and cell surface expression of envelope glycoproteins. *J. Virol.* 73, 1350–1361.

Bonavia, A., Bullock, B. T., Gisselman, K. M., Margulies, B. J., and Clements, J. E. (2005). A single amino acid change and truncated TM are sufficient for simian immunodeficiency virus to enter cells using CCR5 in a CD4-independent pathway. *Virology* 341, 12–23.

Derdeyn, C. A., Decker, J. M., Sfakianos, J. N., Wu, X., O'Brien, W. A., Ratner, L., et al. (2000). Sensitivity of human immunodeficiency virus type 1 to the fusion inhibitor T-20 is modulated by coreceptor specificity defined by the V3 loop of gp120. *J. Virol.* 74, 8358–8367.

DuBridge, R. B., Tang, P., Hsia, H. C., Leong, P. M., Miller, J. H., and Calos, M. P. (1987). Analysis of mutation in human cells by using an Epstein–Barr virus shuttle system. *Mol. Cell. Biol.* 7, 379–387.

Hatada, M., Yoshimura, K., Harada, S., Kawanami, Y., Shibata, J., and Matsushita, S. (2010). Human immunodeficiency virus type 1 evasion of a neutralizing anti-V3 antibody involves acquisition of a potential glycosylation site in V2. *J. Gen. Virol.* 91, 1335–1345.

Haynes, B. F., Gilbert, P. B., Mcelrath, M. J., Zolla-Pazner, S., Tomaras, G. D., Alam, S. M., et al. (2012). Immune-correlates analysis of an HIV-1 vaccine efficacy trial. *N. Engl. J. Med.* 366, 1275–1286.

Hirsch, V. M., Edmondson, P., Murphey-Corb, M., Arbeille, B., Johnson, P. R., and Mullins, J. I. (1989). SIV adaptation to human cells. *Nature* 341, 573–574.

Kodama, T., Wooley, D. P., Naidu, Y. M., Kestler, H. W. III, Daniel, M. D., Li, Y., et al. (1989). Significance of premature stop codons in env of simian immunodeficiency virus. *J. Virol.* 63, 4709–4714.

Kuwata, T., Katsumata, Y., Takaki, K., Miura, T., and Igarashi, T. (2011). Isolation of potent neutralizing monoclonal antibodies from an SIV-Infected rhesus macaque by phage display. *AIDS Res. Hum. Retroviruses* 27, 487–500.

Kuwata, T., Takaki, K., Yoshimura, K., Enomoto, I., Wu, F., Ourmanov, I., et al. (2013). Conformational epitope consisting of the V3 and V4 loops as a target for potent and broad neutralization of simian immunodeficiency viruses. *J. Virol.* 87, 5424–5436.

Kwong, P. D., and Mascola, J. R. (2012). Human antibodies that neutralize HIV-1: identification, structures, and B cell ontogenies. *Immunity* 37, 412–425.

LaBranche, C. C., Sauter, M. M., Haggarty, B. S., Vance, P. J., Romano, J., Hart, T. K., et al. (1995). A single amino acid change in the cytoplasmic domain of the simian immunodeficiency virus transmembrane molecule increases envelope glycoprotein expression on infected cells. *J. Virol.* 69, 5217–5227.

Lusso, P., Cocchi, F., Balotta, C., Markham, P. D., Louie, A., Farci, P., et al. (1995). Growth of macrophage-tropic and primary human immunodeficiency virus type 1 (HIV-1) isolates in a unique CD4+ T-cell clone (PM1): failure to downregulate CD4 and to interfere with cell-line-tropic HIV-1. *J. Virol.* 69, 3712–3720.

Manrique, J. M., Celma, C. C., Affranchino, J. L., Hunter, E., and Gonzalez, S. A. (2001). Small variations in the length of the cytoplasmic domain of the simian immunodeficiency virus transmembrane protein drastically affect envelope incorporation and virus entry. *AIDS Res. Hum. Retroviruses* 17, 1615–1624.

Matsumi, S., Matsushita, S., Yoshimura, K., Javaherian, K., and Takatsuki, K. (1995). Neutralizing monoclonal antibody against a external envelope glycoprotein (gp110) of SIVmac251. *AIDS Res. Hum. Retroviruses* 11, 501–508.

Mori, K., Ringler, D. J., Kodama, T., and Desrosiers, R. C. (1992). Complex determinants of macrophage tropism in env of simian immunodeficiency virus. *J. Virol.* 66, 2067–2075.

Platt, E. J., Wehrly, K., Kuhmann, S. E., Chesebro, B., and Kabat, D. (1998). Effects of CCR5 and CD4 cell surface concentrations on infections by macrophagetropic isolates of human immunodeficiency virus type 1. *J. Virol.* 72, 2855–2864.

Postler, T. S., and Desrosiers, R. C. (2013). The tale of the long tail: the cytoplasmic domain of HIV-1 gp41. *J. Virol.* 87, 2–15.

Reed, L. J., and Muench, H. (1938). A simple method of estimating fifty per cent endpoints. *Am. J. Epidemiol.* 27, 493–497.

Rerks-Ngarm, S., Pitisuttithum, P., Nitayaphan, S., Kaewkungwal, J., Chiu, J., Paris, R., et al. (2009). Vaccination with ALVAC and AIDSVAX to prevent HIV-1 infection in Thailand. *N. Engl. J. Med.* 361, 2209–2220.

Takeuchi, Y., Mcclure, M. O., and Pizzato, M. (2008). Identification of gammaretroviruses constitutively released from cell lines used for human immunodeficiency virus research. *J. Virol.* 82, 12585–12588.

Tamura, K., Peterson, D., Peterson, N., Stecher, G., Nei, M., and Kumar, S. (2011). MEGA5: molecular evolutionary genetics analysis using maximum likelihood, evolutionary distance, and maximum parsimony methods. *Mol. Biol. Evol.* 28, 2731–2739.

Vzorov, A. N., Gernert, K. M., and Compans, R. W. (2005). Multiple domains of the SIV Env protein determine virus replication efficiency and neutralization sensitivity. *Virology* 332, 89–101.

Vzorov, A. N., Weidmann, A., Kozyr, N. L., Khaoustov, V., Yoffe, B., and Compans, R. W. (2007). Role of the long cytoplasmic domain of the SIV Env glycoprotein in early and late stages of infection. *Retrovirology* 4, 94.

Wei, X., Decker, J. M., Liu, H., Zhang, Z., Arani, R. B., Kilby, J. M., et al. (2002). Emergence of resistant human immunodeficiency virus type 1 in patients receiving fusion inhibitor (T-20) monotherapy. *Antimicrob. Agents Chemother.* 46, 1896–1905.

Yoshimura, K., Shibata, J., Kimura, T., Honda, A., Maeda, Y., Koito, A., et al. (2006). Resistance profile of a neutralizing anti-HIV monoclonal antibody, KD-247, that shows favourable synergism with anti-CCR5 inhibitors. *AIDS* 20, 2065–2073.

Yusa, K., Maeda, Y., Fujioka, A., Monde, K., and Harada, S. (2005). Isolation of TAK-779-resistant HIV-1 from an R5 HIV-1 GP120 V3 loop library. *J. Biol. Chem.* 280, 30083–30090.

Yuste, E., Johnson, W., Pavlakis, G. N., and Desrosiers, R. C. (2005). Virion envelope content, infectivity, and neutralization sensitivity of simian immunodeficiency virus. *J. Virol.* 79, 12455–12463.

Yuste, E., Reeves, J. D., Doms, R. W., and Desrosiers, R. C. (2004). Modulation of Env content in virions of simian immunodeficiency virus: correlation with cell surface expression and virion infectivity. *J. Virol.* 78, 6775–6785.

Zhu, P., Chertova, E., Bess, J., Lifson, J. D., Arthur, L. O., Liu, J., et al. (2003). Electron tomography analysis of envelope glycoprotein trimers on HIV and simian immunodeficiency virus virions. *Proc. Natl. Acad. Sci. U.S.A.* 100, 15812–15817.

Zhu, P., Liu, J., Bess, J., Chertova, E., Lifson, J. D., Grisé, H., et al. (2006). Distribution and three-dimensional structure of AIDS virus envelope spikes. *Nature* 441, 847–852.

Conflict of Interest Statement: The authors declare that the research was conducted in the absence of any commercial or financial relationships that could be construed as a potential conflict of interest.

Received: 22 March 2013; accepted: 25 April 2013; published online: 14 May 2013.

*Citation: Kuwata T, Takaki K, Enomoto I, Yoshimura K and Matsushita S (2013) Increased infectivity in human cells and resistance to antibody-mediated neutralization by truncation of the SIV gp41 cytoplasmic tail. Front. Microbiol. **4**:117. doi: 10.3389/fmicb.2013.00117*

This article was submitted to Frontiers in Virology, a specialty of Frontiers in Microbiology.

Bioorganic & Medicinal Chemistry 21 (2013) 2518–2526

Contents lists available at SciVerse ScienceDirect

Bioorganic & Medicinal Chemistry

journal homepage: www.elsevier.com/locate/bmc

CD4 mimics as HIV entry inhibitors: Lead optimization studies of the aromatic substituents

Tetsuo Narumi [a], Hiroshi Arai [a], Kazuhisa Yoshimura [b,c], Shigeyoshi Harada [b,c], Yuki Hirota [a], Nami Ohashi [a], Chie Hashimoto [a], Wataru Nomura [a], Shuzo Matsushita [b], Hirokazu Tamamura [a,*]

[a] Institute of Biomaterials and Bioengineering, Tokyo Medical and Dental University, Chiyoda-ku, Tokyo 101-0062, Japan
[b] Center for AIDS Research, Kumamoto University, Kumamoto 860-0811, Japan
[c] AIDS Research Center, National Institute of Infectious Diseases, Shinjuku-ku, Tokyo 162-8640, Japan

ARTICLE INFO

Article history:
Received 22 January 2013
Revised 25 February 2013
Accepted 26 February 2013
Available online 7 March 2013

Keywords:
CD4 mimicry
Conformational change in gp120
HIV entry inhibitor
Envelope protein opener

ABSTRACT

Several CD4 mimics have been reported as HIV-1 entry inhibitors that can intervene in the interaction between a viral envelope glycoprotein gp120 and a cell surface protein CD4. Our previous SAR studies led to a finding of a highly potent analogue **3** with bulky hydrophobic groups on a piperidine moiety. In the present study, the aromatic ring of **3** was modified systematically in an attempt to improve its antiviral activity and CD4 mimicry which induces the conformational changes in gp120 that can render the envelope more sensitive to neutralizing antibodies. Biological assays of the synthetic compounds revealed that the introduction of a fluorine group as a *meta*-substituent of the aromatic ring caused an increase of anti-HIV activity and an enhancement of a CD4 mimicry, and led to a novel compound **13a** that showed twice as potent anti-HIV activity compared to **3** and a substantial increase in a CD4 mimicry even at lower concentrations.

1. Introduction

The first step of HIV entry into host cells is the interaction of a viral envelope glycoprotein gp120 with the cell surface protein CD4.[1] Such a viral attachment process is an attractive target for the development of the drugs to prevent the HIV-1 infection of its target cells.[2] Several small molecules including BMS-806,[3] IC-9564[4] and NBDs[5] have been identified that inhibit the viral attachment process by binding to gp120. Recently, we and others have been exploring the potentials of NBDs-derived CD4 mimics as a novel class of HIV entry inhibitors (Fig. 1).[6–8]

Small molecular CD4 mimics identified by an HIV syncytium formation assay showed potent cell fusion and virus cell fusion inhibitory activity against several HIV-1 laboratory and primary isolates.[5] Furthermore, the interaction of CD4 mimics with a highly conserved and functionally important pocket on gp120, known as the 'Phe43 cavity', induces conformational changes in gp120,[9] a process which occurs with unfavorable binding entropy, leading to a favorable enthalpy change similar to those caused by binding of the soluble CD4 binding to gp120. These unique properties render CD4 mimics valuable not only for the development of entry inhibitors, but which also, when combined with neutralizing antibodies function as envelope protein openers-putatively, stimulants.[10]

The structure of the complex formed by NBD-556 (**1**) bound to the gp120 core from an HIV-1 clade C strain (C1086) was recently determined by X-ray analysis (PDB: 3TGS).[11] As expected with molecular modeling by us[8a] and others,[6a] NBD-556 binds with Phe43 cavity with its *p*-chlorophenyl ring inserted into the cavity, and in addition multiple contacts were observed, with Trp112, Val255, Phe382, Ile424, Asn425, Trp427, Gly473, and Val430 of gp120 were observed (Fig. 2). However, no obvious interaction with Arg59 of CD4 was observed, although the salt bridge formation between Arg59 of CD4 and Asp368 of gp120 is a critical interaction of the viral attachment.[12] Based on this binding model, several potent compounds were recently identified.[6c,7]

Prior to those studies, we performed structure–activity relationship (SAR) studies based on the modification of the piperidine moiety of CD4 mimics to interact with Val430 and/or Asp368. These resulted in the discovery of a potent compound **3** which has bulky hydrophobic groups on its piperidine ring, and shows significant anti-HIV activity and lower cytotoxicity than other known CD4 mimics.[8c] Our study of the docking of **3** into the Phe43 cavity of gp120 suggests that the cyclohexyl group of **3** can interact hydrophobically with the isopropyl group of Val430.

We hypothesized that the optimization of the aromatic ring of **3** would lead to an increase of antiviral activity and CD4 mimicry, the latter inducing the conformational changes in gp120. Here, we de-

* Corresponding author. Tel.: +81 3 5280 8036; fax: +81 3 5280 8039.
E-mail address: tamamura.mr@tmd.ac.jp (H. Tamamura).

0968-0896/$ - see front matter © 2013 Published by Elsevier Ltd.
http://dx.doi.org/10.1016/j.bmc.2013.02.041

scribe the systematic modification of the aromatic ring of **3** for further optimization to evaluate substituent effects on anti-HIV activity, cytotoxicity and CD4 mimicry.

2. Results and discussion

The co-crystal structure of **1** with the gp120 core revealed that the aromatic group of **1** binds to gp120 by several aromatic–aromatic and hydrophobic interactions (Fig. 2). In particular, hydrophobic space surrounded by the hydrophobic amino acid residues Trp112, Val255, Phe382, and Ile424 is likely to be affected by substituents at the *meta*- and *para*-positions of the aromatic ring, and consequently we decided to investigate substituents at these positions (Fig. 3).

Initially, we selected a chlorine or a methyl group to serve as the *para*-substituent of the aromatic group because CD4 mimic compounds such as **1** (NBD-556) with a *p*-chloro substituent, and because **3** showed significant anti-HIV activity compared to other substituents. Further, CD4 mimic structures such as **2** with a *p*-methyl substituent also showed potent anti-HIV activity and exhibits lower cytotoxicity than those with the *p*-chlorophenyl derivatives.[8a] Next, we chose several halogens including F, Cl and Br, to be the *meta*-substituent on the aromatic group since previous SAR studies revealed that the introduction of an appropriate group with an electron-withdrawing ability at the *meta*-position leads to an increase of binding affinity and antiviral activity.[6a] Furthermore, to investigate whether electron withdrawal and hydrophobicity of the *meta*-position are appropriate, the CD4 mimics with a *meta*-methyl substituent, which has electron-donating properties and is similar in size to bromine, were also synthesized. Finally, two piperidine scaffolds (the 2,2,6,6-tetramethylpiperidine **A** and the dicyclohexylpiperidine **B**) were combined with these aromatics via the oxalamide linker.

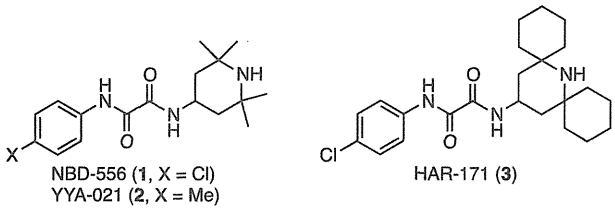

Figure 1. Structures of NBD-556 (**1**), YYA-021 (**2**) and HAR-171 (**3**).

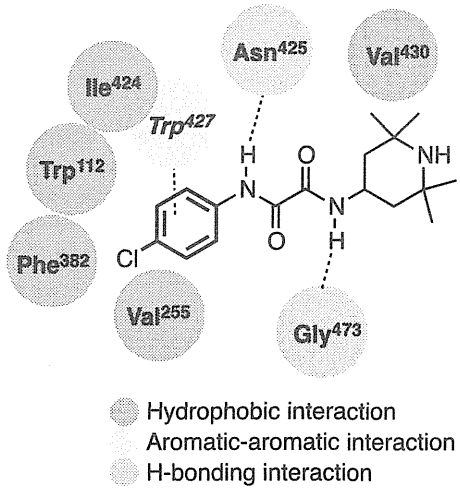

Figure 2. Major interactions between NBD-556 and Phe43 cavity of gp120.

2.1. Chemistry

The syntheses of novel compounds are depicted in Schemes 1 and 2. Starting from the appropriate aniline with *m*- and *p*-substituents, coupling with ethyl chloroglyoxylate in the presence of Et_3N gave the corresponding amidoesters **6a–c** and **7a–c**. Subsequently, microwave-assisted aminolysis[13] of **6a–c** and **7a–c** with commercially available 4-amino-2,2,6,6-tetramethylpiperidines afforded the desired compounds **8a–c** and **9a–c** (Scheme 1). A series of CD4 mimics with two cyclohexyl groups **13a–c** and **14a–c** were prepared from 2,2,6,6-tetramethylpiperidin-4-one **10** by the method previously reported,[8c] with slight modification (Scheme 2). Briefly, treatment of **10** with cyclohexanone in the presence of ammonium chloride gave a 2,6-substituted piperidin-4-one **11** via Grob fragmentation followed by intramolecular cyclization.[14] Reductive amination with *p*-methoxybenzyl amine, acidic treatment with TMSBr/TFA, and oxidative cleavage of *p*-methoxybenzyl group with cerium(IV) ammonium nitrates (CAN) furnished the corresponding 4-aminopiperidines (**12**) with higher yields and less burdensome purifications than the previous method. Finally, coupling of **12** with the corresponding esters **6a–c** and **7a–c** under microwave irradiation provided the desired compounds **13a–c** and **14a–c**.

2.2. Biological evaluation

The anti-HIV activity of the synthetic compounds was evaluated against an R5 primary isolate YTA strain. IC_{50} values were determined by the WST-8 method as the concentrations of the compounds that conferred 50% protection against HIV-1-induced cytopathogenicity in PM1/CCR5 cells. Cytotoxicity of the compounds based on the viability of mock-infected PM1/CCR5 cells was also evaluated using the WST-8 method. The assay results for compounds **8a–c** and **13a–c** with a *p*-chlorophenyl group are shown in Table 1. The parent compound **1** and compound **8a**,[6a] known as JRC-II-191, showed significant anti-HIV activities (IC_{50}

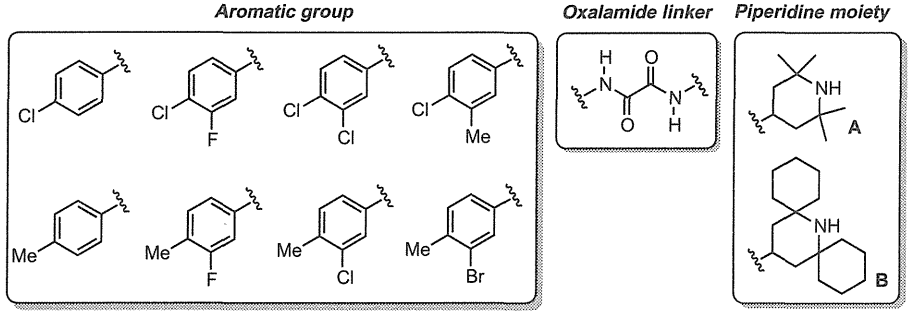

Figure 3. The structures of scaffolds in the design of novel CD4 mimics.

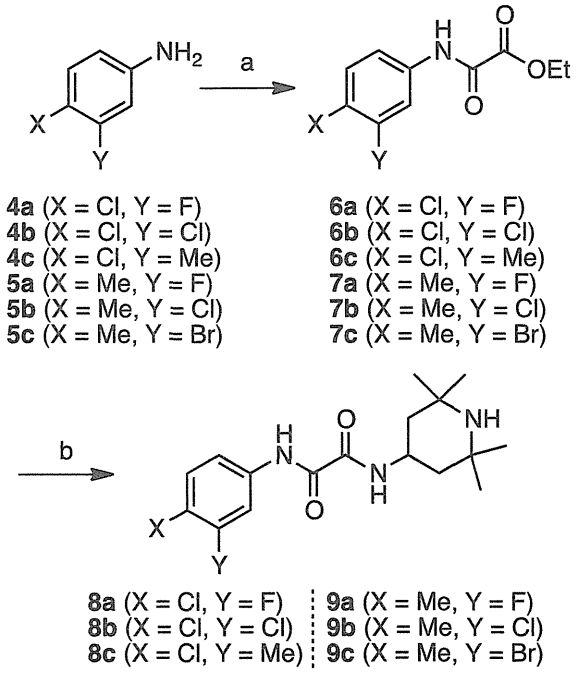

Scheme 1. Reagents and conditions: (a) ethyl chloroglyoxylate, Et_3N, THF; (b) 4-amino-2,2,6,6-tetramethylpiperidine, Et_3N, EtOH, 150 °C, microwave.

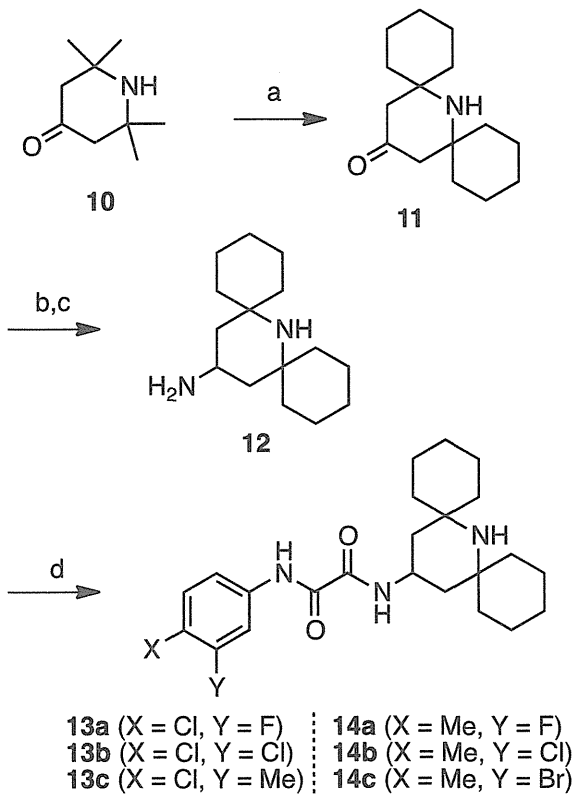

Scheme 2. Reagents and conditions: (a) cyclohexanone, NH_4Cl, DMSO, 60 °C; (b) *p*-methoxybenzylamine, $NaBH_3CN$, MeOH, then 1 M TMSBr in TFA; (c) CAN, CH_3CN/H_2O (v:v = 2:1); (d) **6** or **7**, Et_3N, EtOH, 150 °C, microwave.

of **1** = 0.61 μM and IC_{50} of **8a** = 0.32 μM). Compound **8b**[6a] having a *m,p*-dichlorophenyl group and compound **8c**[6a] (JRC-II-193) having a *p*-chloro-*m*-tolyl group showed moderate anti-HIV activity (IC_{50} of **8b** = 4.1 μM and IC_{50} of **8c** = 3.3 μM) but their potency was

Table 1
Anti-HIV activity and cytotoxicity of compounds **8a–c** and **13a–c** containing a *p*-chlorophenyl group[a]

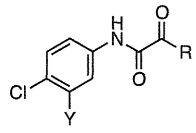

Compd	R	Y	IC_{50}[b] (μM) YTA48P	CC_{50}[c] (μM)
1	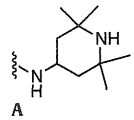	H	0.61	110
8a	**A**	F	0.32	94
8b	**A**	Cl	4.1	36
8c	**A**	Me	3.3	38
3	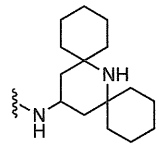	H	0.43	120
13a	**B**	F	0.23	11
13b	**B**	Cl	0.62	11
13c	**B**	Me	2.6	15

[a] All data are the mean values from three of more independent experiments.
[b] IC_{50} values of the multi-round assay are based on the inhibition of HIV-1-induced cytopathogenicity in PM1/CCR5 cells.
[c] CC_{50} values are based on the reduction of the viability of mock-infected PM1/CCR5 cells.

Table 2
Anti-HIV activity and cytotoxicity of compounds **9a–c** and **14a–c** containing a *p*-tolyl group[a]

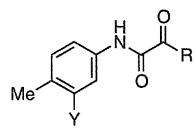

Compd	R	Y	IC_{50}[b] (μM) YTA48P	CC_{50}[c] (μM)
2	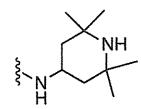	H	9.0	260
9a	**A**	F	2.8	110
9b	**A**	Cl	3.2	62
9c	**A**	Br	>10	32
14a	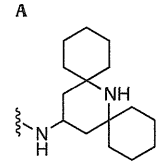	F	0.54	91
14b	**B**	Cl	6.2	11
14c	**B**	Br	3.2	11

[a] All data are the mean values from three of more independent experiments.
[b] IC_{50} values of the multi-round assay are based on the inhibition of HIV-1-induced cytopathogenicity in PM1/CCR5 cells.
[c] CC_{50} values are based on the reduction of the viability of mock-infected PM1/CCR5 cells.

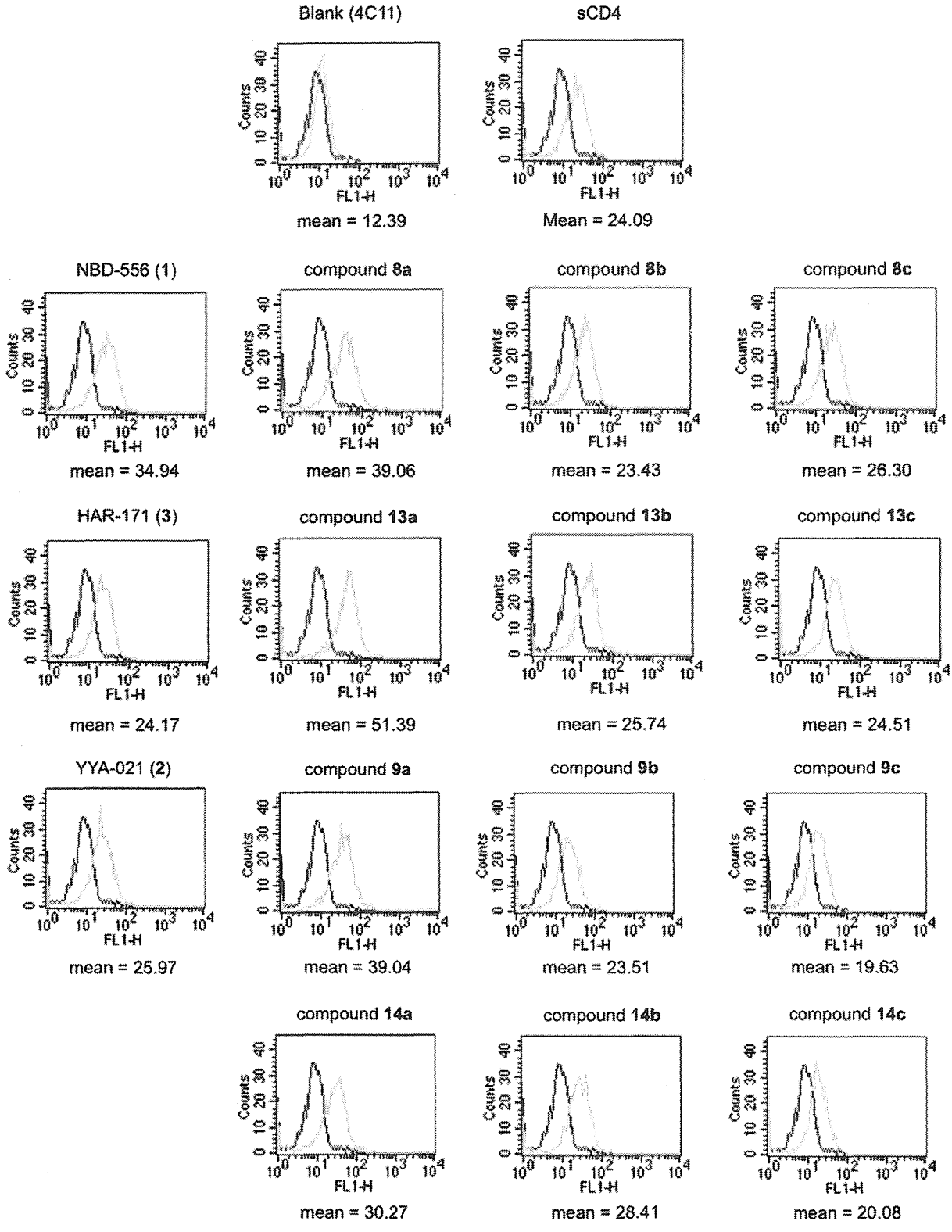

Figure 4. FACS analysis of synthetic compounds **8**, **9**, **13** and **14**.

approximately 10-fold lower than that of compound **8a**. The cytotoxicity of **8b** and **8c** is relatively stronger than that of **8a** (CC_{50} of **8b** = 36 μM and CC_{50} of **8c** = 38 μM). Compounds **13a–c** with hydrophobic cyclohexyl groups in the piperidine moiety showed more potent anti-HIV activity than the corresponding compounds **8a–c**, confirming the contribution of the bulky hydrophobic group(s) to an increase of antiviral activity. Our lead compound **3** showed significant anti-HIV activity comparable to that of compound **8a** (IC_{50} = 0.43 μM) but, consistent with previous results, exhibited lower cytotoxicity. In particular, compound **13a** with a *m*-fluoro-*p*-chlorophenyl group exhibited the highest anti-HIV activity. The IC_{50} value of **13a** was 0.23 μM, whose potency was

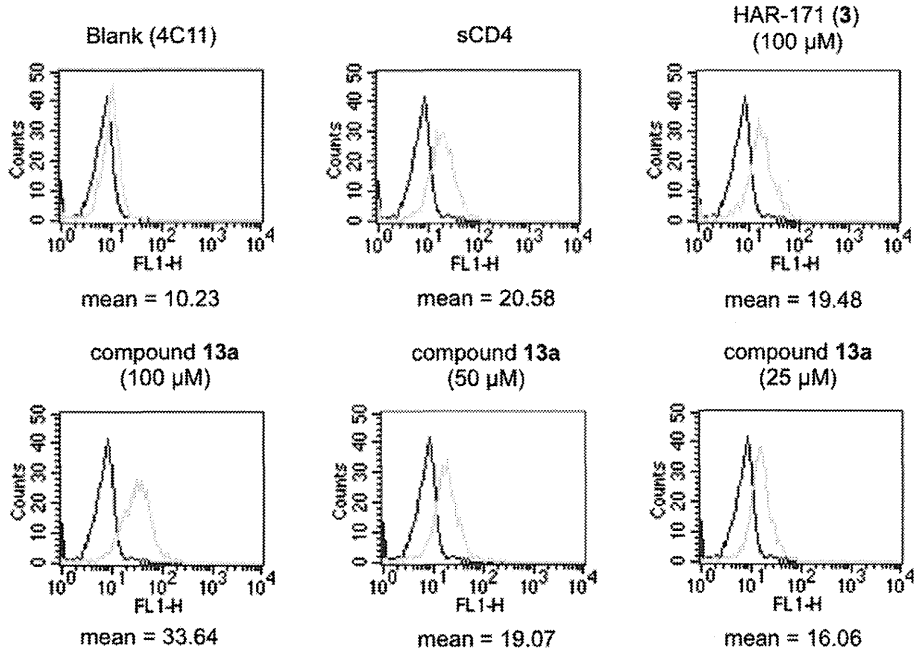

Figure 5. FACS analysis of **3** and **13a** in different concentrations.

approximately twice as high as that of compound **3**. Notably, compound **13b** with a *m,p*-dichlorophenyl group showed 7-fold more potent anti-HIV activity than the corresponding compound **8b**. Compound **13c**, which has a *p*-chloro-*m*-tolyl group, showed potent anti-HIV activity comparable to that of the corresponding compound **8c** and an increase of cytotoxicity (CC_{50} = 15 μM). We observed a tendency for compounds **13a–c** with both hydrophobic cyclohexyl groups and a *m,p*-disubstituted phenyl group to exhibit higher cytotoxicity than the corresponding tetramethyl-type compounds **8a–c**. No clear reason for an increase of cytotoxicity in the *m,p*-disubstituted phenyl group-containing compounds is apparent.

Assay results for the compounds **9a–c** and **14a–c** with a *p*-tolyl group are shown in Table 2. As expected, replacement of the *p*-chloro substituent with a *p*-methyl group resulted in somewhat reduction of anti-HIV activity. Compound **2**, YYA-021 has significant anti-HIV activity (IC_{50} = 9.0 μM) and exhibits the lowest cytotoxicity among all of the compounds tested (CC_{50} = 260 μM). These results are consistent with our previous SAR studies involving the aromatic ring. Introduction of a fluorine at the *meta*-position of the *p*-tolyl group, e.g. in compound **9a** and **14a**, improved the antiviral activity, as observed with **8a** and **13a** and a similar tendency was observed for compound **9b** with a *m*-chloro-*p*-tolyl group. In particular, compound **14a** with cyclohexyl groups and a *m*-fluoro-*p*-tolyl group showed slightly higher anti-HIV activity than the parent compound **1**. Among the compounds with *m*-bromo-*p*-tolyl groups, it was found that compound **9c**, with a 2,2,6,6-tetramethylpiperidine group, showed no anti-HIV activity at a concentration below 10 μM, whereas compound **14c** with hydrophobic cyclohexyl groups attached to the piperidine moiety, showed moderate activity (IC_{50} = 3.2 μM), indicating that the hydrophobic modification of piperidine ring can contribute to an increase in anti-HIV activity.

All the synthetic compounds were evaluated for their CD4 mimicry on the conformational changes in gp120 by fluorescence activated cell sorting (FACS) analysis, and the results are shown in Figure 4. The profile of binding of a CD4-induced (CD4i) monoclonal antibody (4C11) to the Env-expressing cell surface pretreated with the synthetic compounds was assessed in terms of the mean fluorescence intensity (MFI). The increase in binding affinity for 4C11 (by the pretreatment with synthetic compounds) suggests that those compounds can reflect the CD4 mimicry as a consequence of the conformational changes in gp120. Our previous studies disclosed that the profiles of the binding to the cell surface pretreated with **1**, **2**, or **3** were similar to those observed in pretreatment with soluble CD4, indicating that these compounds offer a significant enhancement of binding affinity for 4C11.[8] As shown in Figure 4, similar results were obtained with those compounds in this FACS analysis (MFI of **1**, **2**, and **3** = 34.94, 25.97, and 24.17, respectively). A notable increase in binding affinity for 4C11 was observed in essentially all the synthetic compounds. The compounds **8a**, **9a**, **13a** and **14a** with a *meta*-fluorine in the aromatic ring, showed significant anti-HIV activity, and produced a substantial increase in binding affinity for 4C11. These results suggested that the introduction of a fluorine group at the meta position of the aromatic ring is significant not only for the increase of anti-HIV activity, but also for the enhancement of a CD4 mimicry. In particular, a remarkable improvement in binding affinity for 4C11 was observed with **13a** (MFI = 51.39) which has twofold more potent anti-HIV activity than the lead compound **3** (HAR-171), and is the most active compound in terms of both anti-HIV activity and the CD4 mimicry resulting from the conformational change in gp120. The profiles of pretreatment of the cell surface with compounds **8b** and **13b** having a *m,p*-dichlorophenyl group, compounds **8c** and **13c** having a *p*-chloro-*m*-tolyl group, and compounds **9b** and **14b** with a *m*-chloro-*p*-tolyl group were similar to results obtained for **3**, suggesting that these compounds produced slightly lower enhancement compared to those of compounds **8a**, **9a**, **13a** and **14a** but significant levels of binding affinity for 4C11. On the other hand, pretreatment with compounds **9c**, which failed to show significant anti-HIV activity and **14c**, which had moderate anti-HIV activity resulted in a slight decrease of binding affinity for 4C11, suggesting that the introduction of a Br group at the *meta*-position of *p*-tolyl group is not advantageous to a CD4 mimicry, possibly due to the steric hindrance caused by the two bulky substituents. These results are consistent with previous observations that a limited size and electron-withdrawing ability of the aromatic substituents are required for potent anti-HIV activity and CD4 mimicry.[8a]

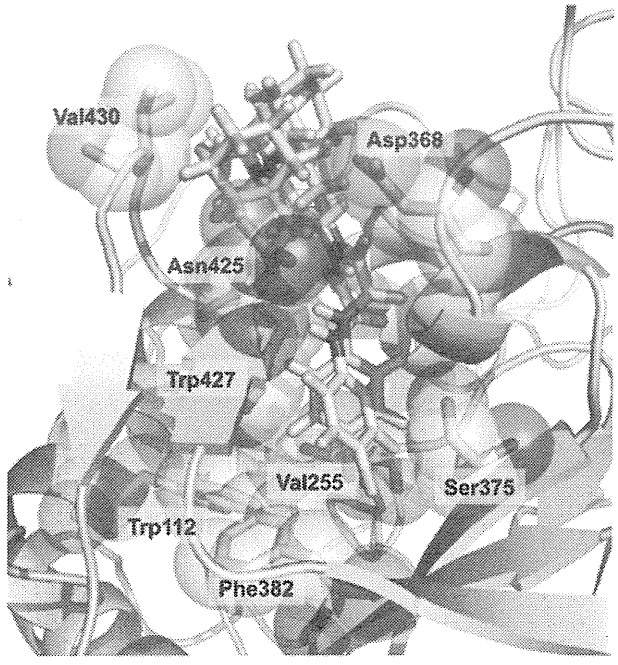

Figure 6. The modeled structure of **13a** (yellow carbon atoms) in the complex with the Phe43 cavity in gp120 (3TGS) overlaid with the modeled structure of **3** (green carbon atoms).

Since **13a** showed higher CD4 mimicry than the other compounds tested, the effect of the solution concentration of **13a** on the binding affinity for 4C11 was investigated. As shown in Figure 5, pretreatment of the cell surface with a 100 μM solution of **13a** produced a higher increase in the binding affinity for 4C11 than pretreatment with the same concentration of compound **3**. Interestingly, the profile pretreated with a 50 μM solution of **13a** was similar to that with a 100 μM of compound **3**, and even with a 25 μM solution of **13a** a potent enhancement of the binding affinity for 4C11 was observed: MFI of **13a** at concentrations of 50 μM and 25 μM = 19.07 and 16.06, respectively. This observation suggests that **13a** could serve as a novel lead compound for the development of envelope protein openers for the use combined with neutralizing antibodies because of its effectiveness at low concentrations.

The substantial increase in the CD4 mimicry of **13a** even at a low concentration is not easily explained because HAR-171 (**3**) and **13a** would be expected to form the similar binding modes with gp120. A probable contribution of **13a** is suggested by modeling studies docked into the Phe43 cavity in gp120 (3TGS) in which the depth and direction of the aromatic ring of **13a** is slightly different from those in compound **3** (Fig. 6), leading to the possible formation of appropriate interactions with the hydrophobic amino acid residues such as Val255 and Phe382, and therefore explaining the increased potency observed in the anti-HIV activity and CD4 mimicry of **13a**.

3. Conclusion

CD4 mimics are attractive agents not only for the development of a novel class of HIV entry inhibitors but also as possible cooperating agents for the neutralizing antibodies—that is, envelope protein openers. In the present study, a structure–activity relationship study of a series of CD4 mimic compounds was performed with a view to improving the biological activity of HAR-171 (**3**), which was identified in our previous studies as a promising lead compound with anti-HIV activity, cytotoxicity and CD4 mimicry resulting from the conformational change in gp120. Systematic modification of the *meta*- and *para*-substituents of the aromatic ring of **3** led to some potent compounds. In particular, **13a**, which has a bulky hydrophobic group on its piperidine ring and a *m*-fluoro-*p*-chlorophenyl group, demonstrated twofold more potent anti-HIV activity and much higher CD4 mimicry than **2** following the conformational changes in gp120, although the cytotoxicity of **13a** is relatively high. Further structural modification studies of the aromatic ring and the oxalamide linker to improve pharmaceutical profiles will be the subject of future reports.

4. Experimentals

^{1}H NMR and ^{13}C NMR spectra were recorded using a Bruker Avance III spectrometer. Chemical shifts are reported in δ (ppm) relative to Me_4Si (in $CDCl_3$) as internal standard. Low- and high-resolution mass spectra were recorded on a Bruker Daltonics microTOF focus in the positive and negative detection mode. For flash chromatography, silica gel 60 N (Kanto Chemical Co., Inc.) was employed. Microwave reactions were performed in Biotage Microwave Reaction Kit (sealed vials) in an Initiator™ (Biotage). The wattage was automatically adjusted to maintain the desired temperature for the desired period of time.

4.1. Chemistry

4.1.1. Ethyl 2-((4-chloro-3-fluorophenyl)amino)-2-oxoacetate (6a)

To a stirred solution of 3-fluoroaniline (1.11 g, 10.0 mmol) in $CHCl_3$ (30.0 mL) was added dropwise *N*-chlorosuccinimide (NCS) in $CHCl_3$ (20.0 mL) at 0 °C. The mixture was stirred at 0 °C for 42 h. After the reaction mixture was concentrated under reduced pressure, the residue was dissolved in Et_2O. The mixture was washed with water, and dried over $MgSO_4$. Concentration under reduced pressure followed by flash chromatography over silica gel with EtOAc/*n*-hexane gave 4-chloro-3-fluoroaniline (259.4 g, 18% yield) as crystalline solids. To a stirred solution of the above aniline (259.4 mg, 1.78 mmol) in THF (8.9 mL) were added at 0 °C ethyl chloroglyoxylate (237.3 μL, 2.14 mmol) and Et_3N (296.6 μL, 2.14 mmol). The mixture was stirred at room temperature for 12 h. After the precipitate was filtrated off, the filtrate solution was concentrated under reduced pressure. The residue was dissolved in EtOAc, and washed with 1.0 M HCl, saturated $NaHCO_3$ and brine, then dried over $MgSO_4$. Concentration under reduced pressure to provide the title compound **6a** (435.2 mg, 99% yield) as brown crystals, which was used without further purification.

^{1}H NMR (500 MHz, $CDCl_3$) δ 1.44 (t, J = 7.50 Hz, 3H), 4.43 (q, J = 7.50 Hz, 2H), 7.24–7.25 (m, 1H), 7.35–7.40 (m, 1H), 7.70–7.75 (m, 1H), 8.93 (br, 1H); ^{13}C NMR (125 MHz, $CDCl_3$) δ 13.0, 64.1, 108.5 (d, J = 26.3 Hz), 115.9 (d, J = 3.75 Hz), 117.3 (d, J = 18.8 Hz), 130.9 (d, J = 10.0 Hz), 135.9, 153.9, 158.1 (d, J = 246.3 Hz), 160.5; HRMS (ESI), m/z calcd for $C_{10}H_{10}ClFNO_3$ (MH^-) 244.0182, found 244.0183.

4.1.2. Ethyl 2-((3,4-dichlorophenyl)amino)-2-oxoacetate (6b)

To a stirred solution of 3,4-dichloroaniline **4b** (1.94 g, 12.0 mmol) in THF (20.0 mL) were added ethyl chloroglyoxylate (1.11 mL, 10.0 mmol) and Et_3N (15.2 mL, 11.0 mmol) at 0 °C. The mixture was stirred at room temperature for 6 h. After the precipitate was filtrated off, the filtrate solution was concentrated under reduced pressure. The residue was dissolved in EtOAc, and washed with 1.0 M HCl, saturated $NaHCO_3$ and brine, then dried over $MgSO_4$. Concentration under reduced pressure to provide the title compound **6b** (1.58 g, 95% yield) as white powder, which was used without further purification.

^{1}H NMR (500 MHz, $CDCl_3$) δ 1.44 (t, J = 7.00 Hz, 3H), 4.43 (q, J = 7.00 Hz, 2H), 7.44 (d, J = 8.50 Hz, 1H), 7.49–7.51 (m, 1H), 7.87, 2.35 (d, J = 2.50 Hz, 1H); ^{13}C NMR (125 MHz, $CDCl_3$) δ 14.0, 64.0, 119.0, 121.5, 129.0, 130.8, 133.2, 135.7, 153.9, 160.5; HRMS (ESI), m/z calcd for $C_{10}H_{10}Cl_2NO_3$ (MH^+) 262.0038, found 262.0031.

4.1.3. Ethyl 2-((4-chloro-3-methylphenyl)amino)-2-oxoacetate (6c)

By use of a procedure similar to that described for the preparation of compound **6b**, the aniline **4c** (3.34 g, 24.0 mmol) was converted into the title compound **6c** (4.63 g, 96% yield) as white powder.

^{1}H NMR (500 MHz, $CDCl_3$) δ 1.43 (t, J = 7.00 Hz, 3H), 2.38 (s, 3H), 4.42 (q, J = 7.00 Hz, 2H), 7.33 (d, J = 8.50 Hz, 1H), 7.43–7.46 (m, 1H), 7.51–7.54 (m, 1H), 8.82 (s, 1H); ^{13}C NMR (125 MHz, $CDCl_3$) δ 14.0, 20.2, 63.8, 118.5, 122.0, 129.7, 130.9, 134.8, 137.1, 153.8, 160.9; HRMS (ESI), m/z calcd for $C_{11}H_{13}ClNO_3$ (MH^+) 242.0578, found 242.0568.

4.1.4. Ethyl 2-((3-fluoro-4-methylphenyl)amino)-2-oxoacetate (7a)

By use of a procedure similar to that described for the preparation of compound **6b**, the aniline **5a** (3.00 g, 24.0 mmol) was converted into the title compound **7a** (4.24 g, 94% yield) as white powder.

^{1}H NMR (500 MHz, $CDCl_3$) δ 1.43 (t, J = 7.20 Hz, 3H), 2.25 (s, 3H), 4.42 (q, J = 6.80 Hz, 2H), 7.12–7.21 (m, 2H), 7.48–7.56 (m, 1H), 8.83 (s, 1H); ^{13}C NMR (125 MHz, $CDCl_3$) δ 14.2 (2C), 63.8, 107.1 (d, J = 27.5 Hz), 115.0 (d, J = 10.0 Hz), 122.3 (d, J = 17.5 Hz), 131.6 (d, J = 6.25 Hz), 135.3 (d, J = 13.8 Hz), 153.8, 160.8, 161.1 (d, J = 243.8 Hz); HRMS (ESI), m/z calcd for $C_{11}H_{13}FNO_3$ (MH^+) 226.0879, found 226.0878.

4.1.5. Ethyl 2-((3-chloro-4-methylphenyl)amino)-2-oxoacetate (7b)

By use of a procedure similar to that described for the preparation of compound **6b**, the aniline **5b** (3.40 g, 24.0 mmol) was converted into the title compound **7b** (5.19 g, 94% yield) as white powder.

^{1}H NMR (500 MHz, $CDCl_3$) δ 1.43 (t, J = 7.00 Hz, 3H), 2.35 (s, 3H), 4.42 (q, J = 7.00 Hz, 2H), 7.22 (d, J = 8.50 Hz, 1H), 7.41–7.43 (m, 1H), 7.71 (d, J = 2.00 Hz, 1H), 8.83 (s, 1H); ^{13}C NMR (125 MHz, $CDCl_3$) δ 14.0, 20.0, 63.8, 118.0, 120.3, 131.2, 133.3, 134.7, 135.0, 153.8, 160.8; HRMS (ESI), m/z calcd for $C_{11}H_{13}ClNO_3$ (MH^+) 242.0584, found 242.0573.

4.1.6. Ethyl 2-((3-bromo-4-methylphenyl)amino)-2-oxoacetate (7c)

By use of a procedure similar to that described for the preparation of compound **6b**, the aniline **5c** (4.47 g, 27.0 mmol) was converted into the title compound **7c** (6.24 g, 96% yield) as white powder.

^{1}H NMR (500 MHz, $CDCl_3$) δ 1.43 (t, J = 7.00 Hz, 3H), 2.38 (s, 3H), 4.42 (q, J = 7.00 Hz, 2H), 7.23 (t, J = 8.50 Hz, 1H), 7.48–7.53 (m, 1H), 7.83–7.90 (m, 1H), 8.80 (s, 1H); ^{13}C NMR (125 MHz, $CDCl_3$) δ 14.0, 22.4, 63.9, 118.7, 123.4, 125.0, 131.0, 135.0, 135.2, 153.7, 160.8; HRMS (ESI), m/z calcd for $C_{11}H_{13}BrNO_3$ (MH^+) 286.0079, found 286.0068.

4.1.7. N^1-(4-Chloro-3-fluorophenyl)-N^2-(2,2,6,6-tetramethylpiperidin-4-yl)oxalamide (8a)

To a solution of compound **6a** (70.0 mg, 0.286) in EtOH (2.9 mL) were added Et_3N (0.200 mL, 1.45 mmol) and 2,2,6,6-tetramethylpiperidin-4-amine (0.150 mL, 0.870 mmol). The reaction mixture was stirred for 3 h at 150 °C under microwave irradiation. After being concentrated in vacuo, the residue was extracted with $CHCl_3$, and washed with saturated $NaHCO_3$ and brine, then dried over $MgSO_4$. Concentration under reduced pressure to provide the title compound **8a** (34.6 mg, 34% yield) as white powder.

^{1}H NMR (500 MHz, $CDCl_3$) δ 0.99–1.50 (m, 15H), 1.92 (dd, J = 3.50, 9.00 Hz, 2H), 4.20–4.32 (m, 1H), 7.21–7.25 (m, 1H), 7.34–7.41 (m, 1H), 7.69–7.73 (m 1H), 9.31 (br, 1H); ^{13}C NMR (125 MHz, $CDCl_3$) δ 28.4, 34.8, 43.8, 44.5, 51.0, 108.3 (d, J = 26.3 Hz), 115.8 (d, J = 3.75 Hz), 117.1 (d, J = 17.5 Hz), 130.8, 136.2 (d, J = 8.75 Hz), 157.6, 158.1 (d, J = 247.5 Hz), 158.4; HRMS (ESI), m/z calcd for $C_{17}H_{24}ClFN_3O_2$ (MH^+) 356.1536, found 356.1548.

4.1.8. N^1-(3,4-Dichlorophenyl)-N^2-(2,2,6,6-tetramethylpiperidin-4-yl)oxalamide (8b)

By use of a procedure similar to that described for the preparation of compound **8a**, the compound **6b** (261.0 mg, 1.00 mmol) was converted into the title compound **8b** (520.0 mg, 70% yield) as white powder.

^{1}H NMR (500 MHz, $CDCl_3$) δ 1.07 (t, J = 12.0 Hz, 2H), 1.16 (s, 6H), 1.28 (s, 6H), 1.90–1.93 (m, 2H), 4.20–4.32 (m, 1H), 7.26 (m, 1H), 7.40–7.48 (m, 2H), 7.88 (s, 1H), 9.33 (s, 1H); ^{13}C NMR (125 MHz, $CDCl_3$) δ 28.5 (2C), 34.9 (2C), 43.8, 44.6 (2C), 50.9 (2C), 119.0, 121.4, 128.7, 130.8, 133.1, 135.8, 157.7, 158.5; HRMS (ESI), m/z calcd for $C_{17}H_{22}Cl_2N_3O_2$ (MH^-) 370.1095, found 370.1105.

4.1.9. N^1-(4-Chloro-3-methylphenyl)-N^2-(2,2,6,6-tetramethylpiperidin-4-yl)oxalamide (8c)

By use of a procedure similar to that described for the preparation of compound **8a**, the compound **6c** (482.0 mg, 2.00 mmol) was converted into the title compound **8c** (364.0 mg, 49% yield) as white powder.

^{1}H NMR (500 MHz, $CDCl_3$) δ 1.07 (t, J = 12.0 Hz, 2H), 1.15 (s, 6H), 1.28 (s, 6H), 1.86–1.94 (m, 2H), 4.15–4.31 (m, 1H), 7.21–7.24 (m, 1H), 7.32–7.38 (m, 2H), 7.74 (s, 1H), 9.24 (s, 1H); ^{13}C NMR (125 MHz, $CDCl_3$) δ 19.6, 28.5 (2C), 34.9 (2C), 43.7, 44.7 (2C), 50.9 (2C), 117.9, 120.2, 131.2, 133.1, 134.7, 135.1, 157.5, 158.8; HRMS (ESI), m/z calcd for $C_{18}H_{25}ClN_3O_2$ (MH^-) 350.1641, found 350.1656.

4.1.10. N^1-(3-Fluoro-4-methylphenyl)-N^2-(2,2,6,6-tetramethylpiperidin-4-yl)oxalamide (9a)

By use of a procedure similar to that described for the preparation of compound **8a**, the compound **7a** (225.0 mg, 1.00 mmol) was converted into the title compound **9a** (161.0 mg, 48% yield) as white powder.

^{1}H NMR (500 MHz, $CDCl_3$) δ 1.07 (t, J = 12.5 Hz, 2H), 1.15 (s, 6H), 1.28 (s, 6H), 1.92 (dd, J = 12.5, 3.50 Hz, 2H), 2.26 (s, 3H), 4.12–4.32 (m, 1H), 7.12–7.20 (m, 2H), 7.30–7.37 (m, 1H), 7.48–7.54 (m, 1H), 9.27 (s, 1H); ^{13}C NMR (125 MHz, $CDCl_3$) δ 14.2, 28.5 (2C), 34.9 (2C), 43.7, 44.7 (2C), 50.9 (2C), 107.1 (d, J = 26.3 Hz), 115.0, 121.8 (d, J = 17.5 Hz) 131.6, 135.4, (d, J = 15.0 Hz), 157.5, 158.8, 161.1 (d, J = 242.5 Hz); HRMS (ESI), m/z calcd for $C_{18}H_{25}FN_3O_2$ (MH^-) 334.1936, found 334.1942.

4.1.11. N^1-(3-Chloro-4-methylphenyl)-N^2-(2,2,6,6-tetramethylpiperidin-4-yl)oxalamide (9b)

By use of a procedure similar to that described for the preparation of compound **8a**, the compound **7b** (482.0 mg, 1.00 mmol) was converted into the title compound **9b** (448.0 mg, 48% yield) as white powder.

^{1}H NMR (500 MHz, $CDCl_3$) δ 1.09 (t, J = 12.5 Hz, 3H), 1.18 (s, 6H), 1.30 (s, 6H), 1.93–1.95 (m, 2H), 2.41 (s, 3H), 4.20–4.34 (m, 1H), 7.30–7.37 (m, 2H), 7.44–7.46 (m, 1H), 7.53 (d, J = 2.50 Hz, 1H), 9.25 (s, 1H); ^{13}C NMR (125 MHz, $CDCl_3$) δ 20.3, 28.5 (2C), 34.9 (2C), 43.7, 44.7 (2C), 50.9 (2C), 118.5, 122.0, 130.0, 130.7, 134.8, 137.1, 157.5, 158.8; HRMS (ESI), m/z calcd for $C_{18}H_{25}ClN_3O_2$ (MH^-) 350.1641, found 350.1636.

4.1.12. N^1-(3-Bromo-4-methylphenyl)-N^2-(2,2,6,6-tetramethylpiperidin-4-yl)oxalamide (9c)

By use of a procedure similar to that described for the preparation of compound **8a**, the compound **7c** (285.0 mg, 1.00 mmol) was converted into the title compound **9c** (157.0 mg, 40% yield) as white powder.

^{1}H NMR (500 MHz, $CDCl_3$) δ 1.07 (t, J = 12.5 Hz, 3H), 1.15 (s, 6H), 1.28 (s, 6H), 1.91 (dd, J = 8.00, 4.00 Hz, 2H), 2.38 (s, 3H), 3.70–3.75 (m, 1H), 7.22 (d, J = 8.50 Hz, 1H), 7.30–7.37 (m, 1H), 7.43–7.45 (m, 1H), 7.90 (d, J = 2.50 Hz, 1H), 9.25 (s, 1H); ^{13}C NMR (125 MHz, $CDCl_3$) δ 22.4, 28.5 (2C), 34.9 (2C), 43.7, 44.7 (2C), 50.9 (2C), 118.6, 123.4, 125.0, 131.0, 134.9 (2C), 157.5, 158.8; HRMS (ESI), m/z calcd for $C_{18}H_{25}BrN_3O_2$ (MH^-) 394.1136, found 394.1158.

4.1.13. Amine (12)

The compound **11** was prepared according to the reported procedure.[14] To a stirred solution of piridone **11** (247.8 mg, 1.05 mmol) in MeOH (2.10 mL) was added *p*-methoxybenzylamine (0.41 mL, 3.15 mmol). After being stirred at room temperature for 23 h, sodium cyanoborohydride was added and stirred at room temperature for 48 h. The reaction mixture was poured into saturated $NaHCO_3$ and extracted with EtOAc, then dried over $MgSO_4$. After concentration under reduced pressure, the residue was treated with 1 M TMS in THF (4.8 mL). The mixture was stirred at 0 °C for 14 h. Concentration under reduced pressure followed by short chromatography with $CHCl_3$/MeOH gave the PMB-protected amine. To a solution of the above amine (584.0 mg, 1.64 mmol) in CH_3CN/H_2O (13.1 mL, v:v = 2:1) was added CAN (2.74 g, 8.2 mmol). The mixture was stirred at room temperature for 14 h. The reaction mixture was diluted with 0.5 M HCl and washed with CH_2Cl_2. The water layer was alkalized and extracted with EtOAc, then dried over Na_2SO_4. Concentration under reduced pressure followed by flash chromatography over silica gel with EtOAc–EtOH (4:1) to gave the title compound **12** (175.5 mg, 71% yield) as a yellow oil.

^{1}H NMR (500 MHz, $CDCl_3$) δ 1.15–1.85 (m, 24H), 2.95–3.05 (m, 1H); ^{13}C NMR (125 MHz, $CDCl_3$) δ 22.2 (2C), 22.8 (2C), 26.2 (2C), 37.3 (2C), 42.3 (2C), 43.6 (2C), 47.0, 53.2 (2C); HRMS (ESI), m/z calcd for $C_{15}H_{29}N_2$ (MH^+) 237.2325, found 237.2321.

4.1.14. N^1-((4-Chloro-3-fluorophenyl)-N^2-(2,6-dicyclohexylpiperidin-4-yl)oxalamide (13a)

By use of a procedure similar to that described for the preparation of compound **8a**, the compound **6a** (36.8 mg, 0.150 mmol) was converted into the title compound **13a** (7.6 mg, 12% yield) as yellow powder.

^{1}H NMR (400 MHz, $CDCl_3$) δ 0.71–2.28 (m, 24H), 2.03–2.20 (m, 2H), 4.02–4.16 (m, 1H), 7.13–7.18 (m, 1H), 7.27–7.33 (m, 1H), 7.62–7.66 (m, 1H), 9.25 (br, 1H); ^{13}C NMR (125 MHz, $CDCl_3$) δ 14.1, 22.0 (2C), 22.6 (2C), 25.8 (2C), 29.3, 29.7 (2C), 31.9, 70.5, 108.3 (d, J = 26.3 Hz), 115.8, 117.1 (d, J = 18.8 Hz), 130.8, 136.2 (d, J = 10.0 Hz), 157.6, 158.1 (d, J = 247.5 Hz), 158.6; HRMS (ESI), m/z calcd for $C_{23}H_{32}ClFN_3O_2$ (MH^+) 436.2162, found 436.2156.

4.1.15. N^1-(4-Chlorophenyl)-N^2-(2,6-dicyclohexylpiperidin-4-yl)oxalamide (13b)

By use of a procedure similar to that described for the preparation of compound **8a**, the compound **6b** (31.3 mg, 0.120 mmol) was converted into the title compound **13b** (28.0 mg, 52% yield) as white powder.

^{1}H NMR (400 MHz, $CDCl_3$) δ 0.96 (t, J = 12.5 Hz, 2H), 1.10–1.84 (br, 20H), 2.05–2.19 (m, 2H), 4.08–4.21 (m, 1H), 7.23–7.33 (br, 1H), 7.39–7.46 (m, 2H), 7.88 (t, J = 1.00 Hz, 1H), 9.34 (s, 1H); ^{13}C NMR (125 MHz, $CDCl_3$) δ 14.1, 22.1 (2C), 22.7 (2C), 26.1 (2C), 31.6, 37.2 (2C), 42.6, 43.0, 43.6, 52.6 (2C), 119.0, 121.4, 128.7, 130.8, 133.1, 135.8, 157.7, 158.5; HRMS (ESI), m/z calcd for $C_{23}H_{32}Cl_2N_3O_2$ (MH^+) 452.1872, found 452.1865.

4.1.16. N^1-((4-Chloro-3-methylphenyl)-N^2-(2,6-dicyclohexylpiperidin-4-yl)oxalamide (13c)

By use of a procedure similar to that described for the preparation of compound **8a**, the compound **6c** (121.0 mg, 0.500 mmol) was converted into the title compound **13c** (15.1 mg, 7% yield) as white powder.

^{1}H NMR (500 MHz, $CDCl_3$) δ 0.87–1.88 (br, 22H), 2.09–2.20 (m, 2H), 2.38 (s, 3H), 4.09–4.22 (m, 1H), 7.32–7.33 (m, 1H), 7.41–7.43 (m, 1H), 7.51 (d, J = 2.00 Hz, 1H), 7.73 (m, 1H), 9.24 (s, 1H); ^{13}C NMR (125 MHz, $CDCl_3$) δ 20.2, 22.1 (2C), 22.7 (2C), 26.0 (2C), 29.7, 37.0, 42.3 (2C), 42.8 (2C), 43.4, 52.9 (2C), 118.4, 122.0, 130.0, 130.6, 134.8, 137.1, 157.5, 158.9; HRMS (ESI), m/z calcd for $C_{24}H_{35}ClN_3O_2$ (MH^+) 430.2267, found 430.2264.

4.1.17. N^1-(3-Fluoro-4-methylphenyl)-N^2-(2,6-dicyclohexylpiperidin-4-yl)oxalamide (14a)

By use of a procedure similar to that described for the preparation of compound **8a**, the compound **7a** (225.0 mg, 1.00 mmol) was converted into the title compound **14a** (27.5 mg, 7% yield) as white powder.

^{1}H NMR (500 MHz, $CDCl_3$) δ 0.971 (t, J = 12.5 Hz, 2H), 1.18–1.86 (m, 20H), 2.13–2.16 (m, 2H), 2.26 (s, 3H), 4.09–4.21 (m, 1H), 7.13–7.18 (m, 2H), 7.33 (d, J = 8.00 Hz, 1H), 7.50–7.53 (m, 1H), 9.27 (s, 1H); ^{13}C NMR (125 MHz, $CDCl_3$) δ 14.2, 22.2 (2C), 22.8 (2C), 26.1 (2C), 37.2 (2C), 42.2 (2C), 43.3 (2C), 43.5, 52.6 (m, 2C), 107.0 (d, J = 27.5 Hz), 115.0 (d, J = 3.75 Hz), 121.8 (d, J = 17.5 Hz), 131.6 (d, J = 6.25 Hz), 135.4 (d, J = 10.0 Hz), 157.5, 158.9, 161.3 (d, J = 242.5 Hz); HRMS (ESI), m/z calcd for $C_{24}H_{33}FN_3O_2$ (MH^-) 414.2554, found 414.2562.

4.1.18. N^1-(3-Chloro-4-methylphenyl)-N^2-(2,6-dicyclohexylpiperidin-4-yl)oxalamide (14b)

By use of a procedure similar to that described for the preparation of compound **8a**, the compound **7b** (120.5 mg, 0.500 mmol) was converted into the title compound **14b** (12.9 mg, 6% yield) as white powder.

^{1}H NMR (500 MHz, $CDCl_3$) δ 0.973 (t, J = 12.5 Hz, 2H), 1.18–1.86 (br, 20H), 2.11–2.19 (m, 2H), 2.35 (s, 3H), 4.09–4.21 (m, 1H), 7.20–7.22 (m, 1H), 7.30–7.32 (m, 1H), 7.35–7.37 (d, J = 2.50 Hz, 1H), 7.73 (m, 1H), 9.22 (s, 1H); ^{13}C NMR (125 MHz, $CDCl_3$) δ 19.6, 22.1 (2C), 22.7 (2C), 26.0 (2C), 29.7, 37.0, 42.1 (2C), 42.7 (2C), 43.2, 53.3 (2C), 118.0, 120.3, 131.2, 133.0, 134.7, 135.1, 157.5, 158.8; HRMS (ESI), m/z calcd for $C_{24}H_{33}ClN_3O_2$ (MH^+) 430.2267, found 430.2257.

4.1.19. N^1-(3-Bromo-4-methylphenyl)-N^2-(2,6-dicyclohexylpiperidin-4-yl)oxalamide (14c)

By use of a procedure similar to that described for the preparation of compound **8a**, the compound **7c** (142.0 mg, 0.500 mmol) was converted into the title compound **14c** (11.5 mg, 5% yield) as white powder.

^{1}H NMR (500 MHz, $CDCl_3$) δ 0.67–2.07 (br, 22H), 2.28 (br, 2H), 2.38 (s, 3H), 4.09–4.21 (m, 1H), 7.22 (d, J = 8.00 Hz, 1H), 7.28–7.38 (br, 1H), 7.43 (dd, J = 4.50, 2.50 Hz, 1H), 7.90 (d, J = 2.50 Hz, 1H), 9.21 (s, 1H); ^{13}C NMR (125 MHz, $CDCl_3$) δ 14.1, 22.1 (2C), 22.4 (2C), 22.7 (2C), 25.9, 30.0, 31.6, 36.9 (2C), 42.7 (3C), 52.7, 52.9, 118.6, 123.4, 125.0, 131.0, 134.9, 135.1, 157.4, 158.8; HRMS (ESI), m/z calcd for $C_{24}H_{33}BrN_3O_2$ (MH^+) 474.1762, found 474.1746.

4.2. Antiviral assay and cytotoxicity assay

Anti-HIV activity and cytotoxicity measurements in PM1/CCR5 cells (Yoshimura et al., 2010) were based on viability of cells that

had been infected or not infected with 100 TCID50 of an R5 primary isolate YTA48P exposed to various concentrations of the test compound. After the PM1/CCR5 cells were incubated at 37 °C for 7 days. The 50% inhibitory concentration (IC_{50}) values and the 50% cytotoxic concentration (CC_{50}) were then determined using the Cell Counting Kit-8 assay (Dojindo Laboratories). All assays were performed in duplicate or triplicate.

4.3. FACS analysis

JR-FL (R5, Sub B) chronically infected PM1 cells were pre-incubated with 0.5 μg/mL of sCD4 or 100 μM of a CD4 mimic for 15 min, and then incubated with an anti-HIV-1 mAb, 4C11, at 4 °C for 15 min. The cells were washed with PBS, and fluorescein isothiocyanate (FITC)-conjugated mouse anti-human IgG antibody was used for antibody-staining. Flow cytometry data for the binding of 4C11 (green lines) to the Env-expressing cell surface in the presence of a CD4 mimic are shown among gated PM1 cells along with a control antibody (anti-human CD19: black lines). Data are representative of the results from a minimum of two independent experiments. The number at the bottom of each graph shows the mean fluorescence intensity (MFI) of the antibody 4C11.

4.4. Molecular modeling

Dockings of compounds **3** and **13a** were performed using Molecular Operating Environment modeling package (MOE 2008. 10, Canada), into the crystal structure of gp120 (PDB, entry 3TGS).

Acknowledgements

This work was supported in part by Grant-in-Aid for Scientific Research from the Ministry of Education, Culture, Sports, Science, and Technology of Japan, and Health and Labour Sciences Research Grants from Japanese Ministry of Health, Labor, and Welfare. We are grateful to Professor Yoshio Hayashi and Dr. Fumika Yakushiji, Tokyo University of Pharmacy and Life Sciences for their assistance in the molecular modelings.

Supplementary data

Supplementary data (NMR charts of compounds) associated with this article can be found, in the online version, at http://dx.doi.org/10.1016/j.bmc.2013.02.041.

References and notes

1. Chan, D. C.; Kim, P. S. *Cell* **1998**, *93*, 681.
2. (a) Kadow, J.; Wang, H.-G.; Lin, P.-F. *Curr. Opin. Investig. Dugs* **2006**, *7*, 721; (b) Repik, A.; Clapham, P. R. *Structure* **2008**, *16*, 1603.
3. Holz-Smith, S.; Sun, I. C.; Jin, L.; Matthews, T. J.; Lee, K. H.; Chen, C. H. *Antimicrob. Agents Chemother.* **2001**, *45*, 60.
4. Lin, P.-F.; Blair, W.; Wang, T.; Spicer, T.; Guo, Q.; Zhou, N.; Gong, Y.-F.; Wang, H.-F. H.; Rose, R.; Yamanaka, G.; Robinson, B.; Li, C.-B.; Fridell, R.; Deminie, C.; Demers, G.; Yang, Z.; Zadjura, L.; Meanwell, N.; Colonno, R. *Proc. Natl. Acad. Sci. U.S.A.* **2003**, *100*, 11013.
5. Zhao, Q.; Ma, L.; Jiang, S.; Lu, H.; Liu, S.; He, Y.; Strick, N.; Neamati, N.; Debnath, A. K. *Virology* **2005**, *339*, 213.
6. (a) Madani, N.; Schön, A.; Princiotto, A. M.; LaLonde, J. M.; Courter, J. R.; Soeta, T.; Ng, D.; Wang, L.; Brower, E. T.; Xiang, S.-H.; Do Kwon, Y.; Huang, C.-C.; Wyatt, R.; Kwong, P. D.; Freire, E.; Smith, A. B., III; Sodroski, J. *Structure* **2008**, *16*, 1689; (b) LaLonde, J. M.; Elban, M. A.; Courter, J. R.; Sugawara, A.; Soeta, T.; Madani, N.; Princiotto, A. M.; Kwon, Y. D.; Kwong, P. D.; Schön, A.; Freire, E.; Sodroski, J.; Smith, A. B., III *Bioorg. Med. Chem. Lett.* **2011**, *20*, 354; (c) LaLonde, J. M.; Kwon, Y. D.; Jones, D. M.; Sun, A. W.; Courter, J. R.; Soeta, T.; Kobayashi, T.; Princiotto, A. M.; Wu, X.; Schön, A.; Freire, E.; Kwong, P. D.; Mascola, J. R.; Sodroski, J.; Madani, N.; Smith, A. B., III *J. Med. Chem.* **2012**, *55*, 4382.
7. Curreli, F.; Choudhury, S.; Pyatkin, I.; Zagorodnikov, V. P.; Bulay, A. K.; Altieri, A.; Kwon, Y. D.; Kwon, P. D.; Debnath, A. K. *J. Med. Chem.* **2012**, *55*, 4764.
8. (a) Yamada, Y.; Ochiai, C.; Yoshimura, K.; Tanaka, T.; Ohashi, N.; Narumi, T.; Nomura, W.; Harada, S.; Matsushita, S.; Tamamura, H. *Bioorg. Med. Chem. Lett.* **2010**, *20*, 354; (b) Narumi, T.; Ochiai, C.; Yoshimura, K.; Harada, S.; Tanaka, T.; Nomura, W.; Arai, H.; Ozaki, T.; Ohashi, N.; Matsushita, S.; Tamamura, H. *Bioorg. Med. Chem. Lett.* **2010**, *20*, 5853; (c) Narumi, T.; Arai, H.; Yoshimura, K.; Harada, S.; Nomura, W.; Matsushita, S.; Tamamura, H. *Bioorg. Med. Chem.* **2011**, *19*, 6735.
9. (a) Schön, A.; Madani, N.; Klein, J. C.; Hubicki, A.; Ng, D.; Yang, X.; Smith, A. B., III; Sodroski, J.; Freire, E. *Biochemistry* **2006**, *45*, 10973; (b) Schön, A.; Lam, S. Y.; Freire, E. *Future Med. Chem.* **2011**, *3*, 1129.
10. Yoshimura, K.; Harada, S.; Shibata, J.; Hatada, M.; Yamada, Y.; Ochiai, C.; Tamamura, H.; Matsushita, S. *J. Virol.* **2010**, *84*, 7558.
11. Kwon, Y. D.; Finzi, A.; Wu, X.; Dogo-Isonagie, C.; Lee, L. K.; Moore, L. R.; Schmidt, S. D.; Stuckey, J.; Yang, Y.; Zhou, T.; Zhu, J.; Vicic, D. A.; Debnath, A. K.; Shapiro, L.; Bewley, C. A.; Mascola, J. R.; Sodroski, J. G.; Kwong, P. D. *Proc. Natl. Acad. Sci. U.S.A.* **2012**, *109*, 5663.
12. (a) Kwong, P. D.; Wyatt, R.; Robinson, J.; Sweet, R. W.; Sodroski, J.; Hendrickson, W. A. *Nature* **1998**, *393*, 648; (b) Kwong, P. D.; Wyatt, R.; Mcajeed, S.; Robinson, J.; Sweet, R. W.; Sodroski, J.; Hendrickson, W. A. *Structure* **2000**, *8*, 1329.
13. McFarland, C.; Vicic, D. A.; Debnath, A. K. *Synthesis* **2006**, 807.
14. Sakai, K.; Yamada, K.; Yamasaki, T.; Kinoshita, Y.; Mito, F.; Utsumi, H. *Tetrahedron* **2010**, *66*, 2311.

JVI
Journals.ASM.org

Conformational Epitope Consisting of the V3 and V4 Loops as a Target for Potent and Broad Neutralization of Simian Immunodeficiency Viruses

Takeo Kuwata,[a] Kaori Takaki,[a] Kazuhisa Yoshimura,[b] Ikumi Enomoto,[a] Fan Wu,[c] Ilnour Ourmanov,[c] Vanessa M. Hirsch,[c] Masaru Yokoyama,[d] Hironori Sato,[d] Shuzo Matsushita[a]

Center for AIDS Research, Kumamoto University, Kumamoto, Japan[a]; AIDS Research Center, National Institute of Infectious Diseases, Tokyo, Japan[b]; Laboratory of Molecular Microbiology, NIAID, NIH, Bethesda, Maryland, USA[c]; Pathogen Genomics Center, National Institute of Infectious Diseases, Tokyo, Japan[d]

Inducing neutralizing antibodies (NAb) is the key to developing a protective vaccine against human immunodeficiency virus type 1 (HIV-1). To clarify the neutralization mechanism of simian immunodeficiency virus (SIV), we analyzed NAb B404, which showed potent and broad neutralizing activity against various SIV strains. In 4 SIVsmH635FC-infected macaques, B404-like antibodies using the specific VH3 gene with a long complementarity-determining region 3 loop and λ light chain were the major NAbs in terms of the number and neutralizing potency. This biased NAb induction was observed in all 4 SIVsmH635FC-infected macaques but not in 2 macaques infected with a SIV mix, suggesting that induction of B404-like NAbs depended on the inoculated virus. Analysis using Env mutants revealed that the V3 and V4 loops were critical for B404 binding. The reactivity to the B404 epitope on trimeric, but not monomeric, Env was enhanced by CD4 ligation. The B404-resistant variant, which was induced by passages with increasing concentrations of B404, accumulated amino acid substitutions in the C2 region of gp120. Molecular dynamics simulations of the gp120 outer domains indicated that the C2 mutations could effectively alter the structural dynamics of the V3/V4 loops and their neighboring regions. These results suggest that a conformational epitope consisting of the V3 and V4 loops is the target for potent and broad neutralization of SIV. Identifying the new neutralizing epitope, as well as specifying the VH3 gene used for epitope recognition, will help to develop HIV-1 vaccines.

Neutralizing antibodies (NAb) against human immunodeficiency virus type 1 (HIV-1) protect against viral challenge in nonhuman primate models (1–5), suggesting that NAb induction may be an important key to the development of vaccines against HIV-1. The role of NAbs in prevention of infection and control of viral replication has been suggested in several studies using candidate vaccines (6–8). However, the difficulties in inducing NAbs, especially those that are broadly reactive to various HIV-1 strains, have hampered the development of such vaccines (9–11). Monoclonal antibodies (MAb) with broad neutralizing activity that were recently isolated from HIV-1-infected patients have been characterized to understand the specificities and mechanisms of broad neutralization (12–16). The epitopes of these potent and broad NAbs, such as PG9, PGT128, VRC01, and 10E8, have been determined precisely (17–19) and provide an opportunity for structure-based vaccine design to develop antibody-based vaccines for HIV-1 (11, 20–23).

Nonhuman primate models of simian immunodeficiency virus (SIV) infection are commonly used to develop vaccines against HIV-1 (6, 8, 24). Various immunogens, vectors, and regimens have been evaluated by challenge infection with SIV. Moreover, immune factors associated with prevention of infection have been explored in the SIV model. However, epitopes for potent and broad neutralization of SIV remain unclear because few MAbs that neutralize a wide range of SIV strains have been available. Recently, we isolated MAbs from a rhesus macaque infected with SIVsmH635FC, which was isolated from a rapid progressor macaque (25). Infection with SIVsmH635FC, a highly neutralization-sensitive molecular clone, resulted in a vigorous and potent antibody response in all the infected macaques together with viral mutations to escape antibody recognition (26, 27). MAb B404 bound to a conformational epitope on gp120 of various SIV strains and did not react to overlapping peptides of SIV Env. The V3 region was shown to be important by competition enzyme-linked immunosorbent assay (ELISA) with anti-V3 antibodies (25). The neutralizing activity of B404 against homologous neutralization-sensitive SIVsmH635FC, genetically divergent SIVmac316, and neutralization-resistant SIVsmE543-3 was observed.

In this study, we analyzed the epitope of B404 and the induction of B404-like NAbs in SIV-infected macaques. Analysis of more than 400 anti-Env MAbs demonstrated that B404-like NAbs with the same gene usage and specificity were mainly induced in 4 SIVsmH635FC-infected macaques. The B404 epitope was mapped to a conformational epitope consisting of the V3 and V4 loops exposed on a trimeric Env structure after CD4 binding. The identification of the new neutralizing epitope and vigorous antibody response to this epitope in SIV-infected macaques will help us to understand broad neutralization in a macaque model of SIV infection.

MATERIALS AND METHODS

Cells and viruses. PM1 (28) and PM1/CCR5 (29) cells were maintained in RPMI 1640 medium containing 10% fetal bovine serum (FBS). TZM-bl

Received 22 January 2013 Accepted 25 February 2013
Published ahead of print 6 March 2013
Address correspondence to Shuzo Matsushita, shuzo@kumamoto-u.ac.jp.

doi:10.1128/JVI.00201-13

(30–33) and 293T (34) cells were maintained in Dulbecco's modified Eagle medium containing 10% FBS. Infectious molecular clones, SIVsmE543-3 (35), SIVsmH635FC (27), SIVmac239 (36), SIVmac316 (37), SIVsmE660FL14, SIVsmH805-24w-3, and SIVsmH807-24w-4 (38) were transfected into 293T cells. After 2 days, the supernatants were filtered (0.45 μm) and stored at −80°C as virus stocks.

Construction of Fab libraries from SIV-infected macaques. The Fab library from SIVsmH635FC-infected rhesus macaque H723 was described previously (25). The Fab libraries from SIV-infected rhesus macaques H704, H709, H714, H711, and H725 (26, 27, 39) were similarly constructed using the pComb3X system according to the instructions of Barbas et al. (40). Four macaques, H723, H704, H709, and H714, were infected with SIVsmH635FC. H711 was infected with a combination of SIVsmE543-3 and SIVsmH635FC. H725 was infected with plasma samples from 2 SIVsmH445-infected macaques, H631 and H635. Rhesus macaques of Indian origin were used in this study. RNA was extracted from lymphocytes from the lymph nodes of these macaques using an RNeasy minikit (Qiagen, Hilden, Germany) and used for subsequent RT-PCR using oligo(dT)20 primer, ReverTra Ace (Toyobo, Osaka, Japan), and Platinum high-fidelity *Taq* DNA polymerase (Invitrogen, Carlsbad, CA). Two libraries, κ and λ light chains, were constructed for each macaque to examine the frequency of NAbs in each population, although only one library, containing both κ and λ light chains, was constructed for H723. Immunoglobulin (Ig) genes were inserted into pComb3X, and the ligation mix was used for transformation of XL1-Blue (Stratagene, La Jolla, CA) by electroporation. Transformed cultures were incubated in superbroth medium with 50 μg/ml carbenicillin, 10 μg/ml tetracycline, and 1.4 μg/ml kanamycin overnight at 37°C after addition of VCSM13 helper phage (Stratagene). Library phage stock was obtained from the culture medium by polyethylene glycol 8000–NaCl precipitation. Library size was determined by assessing the number of CFU after infection of XL1-Blue with a diluted phage sample.

Biopanning to obtain anti-Env antibodies. Biopanning was performed using SIV antigen (Ag), which was prepared by infection of PM1 cells with SIVsmE543-3 as previously described (25). To obtain Fab clones against Env, we selected Fab clones from the H723 library using a 96-well plate in which Env was conjugated with anti-Env Fab clones B404, B408, and H301, which recognize gp120 (conformational), gp41 cluster I and gp120 V1, respectively (25). A MaxiSoap 96-well plate (Thermo Fisher Scientific, Waltham, MA) was incubated with 100 μl of 1.25 μg/ml B404, 0.625 μg/ml B408, and 10 μg/ml H301 for 1 h at 37°C. The wells were washed with phosphate-buffered saline (PBS) containing 0.05% Tween 20 (PBS-T) and blocked with 5% skim milk (Wako Pure Chemical Industries, Osaka, Japan) in PBS (MPBS) for 1 h at 37°C. After the blocking solution was discarded, the wells were incubated with 100 μl 40-fold-diluted SIV Ag for 1 h at 37°C, washed with PBS-T, and used for panning. After incubation with 50 μl of phage library for 2 h at 37°C, the wells were washed 5 times with PBS-T, and bound phage was eluted with 50 μl 100 mM glycine (pH 2.2). Amplified phage was used for the next round of panning, and 3 or 4 rounds of panning were performed. To isolate Fab clones specific to Env, we transformed phagemid DNA into TOP10F′ *Escherichia coli* cells (Invitrogen), and supernatants from isopropyl-β-D-thiogalactopyranoside (IPTG; Wako Pure Chemical Industries)-induced cultures were screened for reactivity to SIV Env using ELISA. Fab clones were purified using a His GraviTrap column (GE Healthcare, Buckinghamshire, United Kingdom), as described previously (25).

Construction of a single-chain variable fragment (scFv) form of B404. B404 Fab was previously converted into complete rhesus IgG produced from a stable cell line carrying heavy- and light-chain plasmids pHCG-B404 and pLL-B404 (25). From these plasmids, B404 scFv was constructed using the pComb3X system (40). The heavy-chain variable region (VH) was amplified using pHCG-B404 as a template and primers HSCVH35-FL (5′-GGT GGT TCC TCT AGA TCT TCC TCC TCT GGT GGC GGT GGC TCG GGC GGT GGT GGG GAG GTG CAG CTG GTG SAG TCT GG-3′) and RhSCG404-B (5′-CCT GGC CGG CCT GGC CAC TAG TGA CCG ATG GGC CCT TGG TGG AGC C-3′). The light-chain λ variable region (VL) was amplified from pLL-B404 using primers HSCLam3 (5′-GGG CCC AGG CGG CCG AGC TCG AGC TGA CTC AGC CAC CCT CAG TGT C-3′) and RhSCJLam404 (5′-GGA AGA TCT AGA GGA ACC ACC GCC TAG GAC GGT CAG CCG GGT CCC-3′). The amplified products were combined by overlapping PCR using primers RSC-F (5′-GAG GAG GAG GAG GAG GAG GCG GGG CCC AGG CGG CCG AGC TC-3′) and RSC-B (5′-GAG GAG GAG GAG GAG GAG CCT GGC CGG CCT GGC CAC TAG TG-3′), digested with SfiI, and inserted into pComb3X in a manner similar to that of Fab construction. The resultant plasmid had the B404 VL and VH regions, which were connected with an 18-amino-acid linker, a histidine tag, and a hemagglutinin (HA) tag. This plasmid was transformed into Rosetta 2 (Merck, Darmstadt, Germany), and B404 scFv was purified from the cell pellet using a His GraviTrap column.

ELISA. ELISA was performed to detect antibodies specific to SIV Ag as previously described (25, 41). Briefly, a MaxiSoap 96-well plate was coated with PBS containing 50 ng/ml concanavalin A (Sigma, St. Louis, MO) for 1 h at 37°C, and SIV Env was conjugated by incubation with 50 μl/well 10-fold diluted SIV Ag for 1 h at 37°C. Samples were added to each well at 50 μl/well with 50 μl of MPBS, and the plate was incubated for 1 h at 37°C. When the enhancement effect of soluble CD4 (sCD4) was examined, 25 μl of sample, 25 μl of sCD4, and 50 μl MPBS were added to each well. Fabs specific to SIV Env were detected with anti-HA–peroxidase (1:1,000 dilution; 3F10, Roche Molecular Biochemicals, Mannheim, Germany) and ABTS [2,2′-azinobis(3-ethylbenzthiazolinesulfonic acid)] solution (Roche Molecular Biochemicals).

Competition ELISA was performed similarly using B404 IgG as a competitor. Ag-coated wells were incubated with 50 μl MPBS and 25 μl serial dilutions of B404 IgG for 1 h at 37°C. After incubation with 25 μl subsaturating concentrations of Fab clones, Fab clone binding was detected by anti-HA–peroxidase (1:1,000) and ABTS solution.

Analysis of neutralizing antibody titers. The neutralizing capability of Fab samples was measured as the reduction in luciferase activity after infection of TZM-bl cells with various SIV strains (6, 25). In addition to Fab samples, plasma samples from SIVsmH635FC-infected macaque H704 (26) and SIVmac239-infected macaque MM324 (42) and MAb M318T (43), which recognizes the V2 region of SIV Env, were used to examine the sensitivity of SIV variants to antibody-mediated neutralization. Briefly, 100-μl portions of serially diluted samples in duplicate were incubated with 50 μl containing 200 50% tissue culture infectious doses ($TCID_{50}$) of virus in a 96-well plate. After incubation for 1 h at 37°C, 100 μl containing 1×10^5 TZM-bl cells/ml with 37.5 μg/ml DEAE dextran was added. Infected cultures were incubated for 2 days, but cultures infected with SIVsmH635FC were incubated for 3 days. After incubation, cells were lysed with 30 μl cell lysing buffer (Promega, Madison, WI) for 15 min at room temperature (RT), and 10 μl cell lysate was transferred to a 96-well black solid plate (OptiPlates-96F; Perkin-Elmer, Boston, MA) for measurements of luminescence using a GloMax 96 microplate luminometer (Promega) and a luciferase assay system (Promega). The 50 and 90% inhibitory concentrations (IC_{50} and IC_{90}, respectively) were calculated with nonlinear regression using PRISM5 and defined as the concentration that caused 50 and 90% reductions in luciferase activity, respectively, compared to that in virus control wells after the subtraction of background.

Construction of Env mutants. The *env* gene was amplified by PCR using primers SRev-F (5′-GGT TTG GGA ATA TGC TAT GAG-3′) and SEnv-R (5′-CCT ACT AAG TCA TCA TCT T-3′) and SIVsmE543-3 plasmid as a template. The PCR product was inserted into pcDNA3.1/V5-His-TOPO vector (Invitrogen). After XbaI digestion, the plasmid was ligated with an NheI-XbaI fragment from pLP-IRES2-EGFP (Clontech Laboratories Inc., Mountain View, CA) to generate a plasmid designated RE543-EGFP that expressed both enhanced green fluorescent protein (EGFP) and Env. Mutants were constructed from RE543-EGFP using PCR mutagenesis. Deletion mutants ΔV1, ΔV2, ΔV3, and ΔV4 were created by

deleting amino acid residues 115 to 149 in the V1 loop, 153 to 209 in the V2 loop, 313 to 342 in the V3 loop, and 404 to 430 in the V4 loop and replacing them with Gly-Ala-Gly, Gly, Gly-Ala, and Gly-Ala-Gly, respectively. These mutations were introduced into RE543-EGFP using primers DV1F (5′-ATG TAA TGG AGC CGG CTC TTG CAT AAA AAA-3′) and DV1R (5′-AAG AGC CGG CTC CAT TAC ATC TCA TTG CTA-3′) for ΔV1, DV2F (5′-ATA GGA GCC GGC CAT TGT AAC ACC AGT-3′) and DV2R (5′-ACA ATG GCC GGC TCC TAT GCA AGA ATC ACC-3′) for ΔV2, DV3F (5′-TGT AGA GGA GCC GGC TGG TGC CGG TTT GGA-3′) and DV3R (5′-GCA CCA GCC GGC TCC TCT ACA TTT CAT TGT-3′) for ΔV3, and DV4F (5′-AAG AAT TCT TAT ACT GCA AAG GAG CCG GCC CAT GTC ATA TTA GAC AAA-3′) for ΔV4. Mutant ΔGly was constructed using primers N306AFw2 (5′-TAT TAT GCT CTA ACA ATG AAA TGT AG-3′), N306ARv (5′-CAT TGT TAG AGC ATA ATA CTT-3′), N316AFw (5′-AGA CCA GGA GCT AAG ACA GTT-3′), N316ARv (5′-AAC TGT CTT AGC TCC TGG TCT-3′), N349AFw (5′-GGT TTG GAG GAG CCT GGA GCG-3′), and N349ARv (5′-CGC TCC AGG CTC CTC CAA ACC G-3′) to introduce the mutations N306A, N316A, and N349A at potential N-linked glycosylation sites. Mutant D385R was constructed using primers S-D368RFw (5′-CCA GCA GGA GGA CGT CCA GAA GTC AC-3′) and S-D368RRv (5′-TTC TGG ACG TCC TCC TGC TGG AGC TGT-3′). The D385R substitution in SIVsmE543-3 corresponds to D368R in HIV-1, which interferes with CD4 binding site (CD4bs) antibodies (13, 44, 45). Mutant I434R was constructed using primers S-I420RFw (5′-GCC ATG TCA TCG TAG ACA AAT AAT CAA C −3′) and S-I420RRv (5′-GAT TAT TTG TCT ACG ATG ACA TGG CAC −3′). The I434R substitution in SIVsmE543-3 corresponds to I420R in HIV-1, which interferes with CD4-induced (CD4i) antibodies (13, 45, 46). Amino acid numbering of Env was based on that of SIVmac239, the reference sequence of SIV, and the HIV-2 sequence in the Los Alamos HIV databases (http://www.hiv.lanl.gov/).

Flow-cytometric analysis. Plasmids to express wild-type and mutant Env were transfected into 293T cells using X-tremeGENE 9 DNA transfection reagent (Roche Molecular Biochemicals) according to the manufacturer's instructions. After incubation for 2 days, the transfected cells were detached with PBS containing 0.05% trypsin and 0.53 mM EDTA and adjusted to 1×10^7 cells/ml in PBS containing 0.2% bovine serum albumin (BSA). To examine the reactivity of Fab, we incubated 50 μl cells with 10 μl 50 ng/μl Fab for 40 min at RT. After washing with PBS containing 0.2% BSA, the cells were incubated with 50 μl anti-HA antibody (1:200; 3F10; Roche Molecular Biochemicals) for 20 min at RT, followed by incubation with 50 μl allophycocyanin (APC)-conjugated AffiniPure goat anti-rat IgG (H+L) $F(ab')_2$ fragment (1:200; Jackson ImmunoResearch Laboratories, Inc., West Grove, PA) for 20 min at RT. When enhancement with sCD4 was examined, cells were resuspended in PBS containing 0.2% BSA in the presence or absence of 2 μg/ml sCD4 at 1×10^7 cells/ml before staining. After incubation with sCD4 for 15 min at RT, 20 μl of cells was mixed with 10 μl 25 ng/μl Fab and stained with anti-HA and anti-rat antibodies. Murine MAb KK46 (1:200) was used as a control antibody against the linear V3 epitope (47). KK46-incubated cells were stained by APC-conjugated goat anti-mouse Ig (1:200; BD Biosciences, Franklin Lakes, NJ). The stained cells were analyzed using a FACSCalibur flow cytometer (BD Biosciences). The reactivity of Fab to Env was determined by comparison with an unstained control after gating $EGFP^+$ cells. Data analysis was performed using FlowJo (TreeStar, San Carlos, CA).

Isolation of B404-resistant variants from SIVmac316. The selection of B404-resistant variants from SIVmac316 was performed as described previously (48, 49). Briefly, 5,000 $TCID_{50}$ SIVmac316 was incubated with 5 ng/ml Fab B404 for 30 min at 37°C. Then, 5×10^4 PM1/CCR5 cells were added to the virus-Fab mixture. After incubation for 5 h, cells were washed with PBS and resuspended in RPMI 1640 medium supplemented with 10% FBS without Fab B404. The culture supernatant was harvested on day 7 and used to infect fresh PM1/CCR5 cells for the next round of culture in the presence of increasing concentrations of Fab B404. A B404-resistant virus, P26B404, was recovered from the cell culture supernatant at passage 26 at 400 μg/ml Fab B404. SIVmac316 was also passaged for the same period in PM1/CCR5 cells in the absence of Fab B404, and the resulting virus was designated P26C. Proviral DNA samples were extracted from PM1/CCR5 cells infected with P26B404 and P26C using a QIAamp DNA blood minikit (Qiagen). The gp120 region was amplified by PCR using primers SEnv-F (5′-ATG GGA TGT CTT GGG AAT CAG C-3′) and SER1 (5′-CCA AGA ACC CTA GCA CAA AGA CCC-3′), cloned using a TA cloning kit (Invitrogen), and subjected to sequencing.

Nucleic acid sequence analysis. The Ig variable regions were sequenced using the primers ompseq and pelseq (40), and analyzed with V-QUEST in the International Immunogenetics Database (IMGT; http://www.imgt.org/) (50). The germ line sequence of the VH gene, from which B404 originated, was determined using the genome database of rhesus macaque (51). Sequences were aligned and phylogenetically analyzed using Molecular Evolutionary Genetics Analysis version 5 (MEGA5) (52).

The gp120 region from P26B404 and P26C was sequenced using primers M13F and M13R in the vector and SE1 (5′-ATA ATA CAG TCA CAG AAC A-3′). Predicted amino acid sequences were aligned using CLC Sequence Viewer 6 (CLC Bio, Aarhus, Denmark), together with other SIV sequences.

Molecular dynamics (MD) simulation of gp120 from B404-resistant variants. MD simulations of the gp120 outer domain of SIVmac316 and the mutants with a F277V or N295S substitution were performed essentially as described for MD simulations of the HIV-1 gp120 outer domain (53). SIV gp120 outer domain structures with various V3 regions were constructed using the homology modeling technique with the Molecular Operating Environment (MOE) 2011.10 (Chemical Computing Group Inc., Montreal, Quebec, Canada). The modeling template was the crystal structure of HIV-1 gp120 containing the entire V3 region at a resolution of 3.30 Å (PDB code, 2QAD [54]) and the SIV gp120 core at a resolution of 4.00 Å (PDB code, 3FUS [55]). The 195 amino-terminal and 7 carboxyl-terminal residues were deleted to construct the gp120 outer domain structures. Glycans were added to the gp120 outer domain structures using Online Glycoprotein Builder (56). MD simulations were performed using the SANDER module in the AMBER 10 program package (57, 58) and the AMBER force field (59) and GLYCAM06 (60) with the TIP3P water model (61). Bond lengths involving hydrogen were constrained with SHAKE (62), and the time step for all MD simulations was set to 2 fs. A nonbonded cutoff of 12 Å was used. After heating calculations for 20 ps until 310 K using the NVT ensemble, the simulations were executed using the NPT ensemble at 1 atm and at 310 K for 50 ns. To map structurally fluctuating sites in the gp120 outer domain, we calculated the root mean square fluctuation (RMSF) of the main chains of individual amino acid residues as described previously (53). Briefly, the RMSF were calculated using the 90,000 snapshots obtained from MD simulations of 5 to 50 ns. The average structures during these MD simulations were used as reference structures for the calculation of the RMSF using the ptraj module in AMBER 10.

Nucleotide sequence accession numbers. Sequence data for Ig clones obtained from SIVsmH635FC-infected macaques were submitted to GenBank under accession numbers JF925337 to JF925378 and JF925380 to JF926116.

RESULTS

Potent and broad neutralizing activity of NAb B404 against various SIV strains. SIV-specific Fab clones were previously isolated from the Fab library from SIVsmH635FC-infected macaque H723 through panning against whole SIV Ag (25). Four Fab clones specific to gp120, represented by B404, showed similar gene usage, epitope specificity, and neutralizing activity that covered homologous and heterologous SIV strains. To define the neutralizing potency of B404 further, IgG, Fab, and scFv with B404 variable regions were constructed and examined for their neutralizing ac-

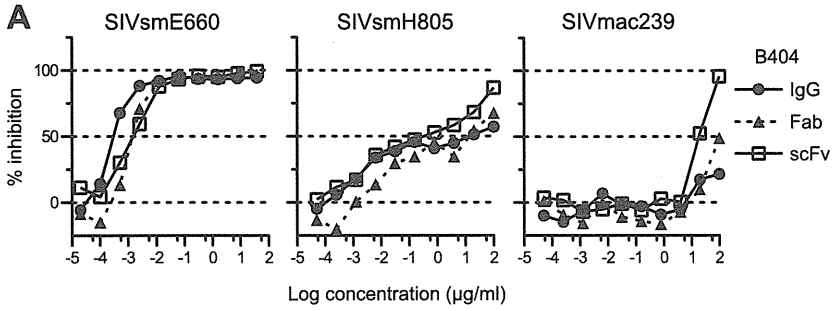

B

IC_{50} and IC_{90}(μg/ml) of IgG, Fab and scFv of B404 against various SIV strains.

Virus	% aa difference	IgG		Fab		scFv	
		IC50	IC90	IC50	IC90	IC50	IC90
SIVmac316	16.8	2.5E-04	1.9E-03	6.0E-04	4.8E-03	4.5E-04	1.9E-03
SIVsmE660	7.3	3.0E-04	2.5E-03	1.4E-03	7.8E-03	1.6E-03	2.0E-02
SIVsmH635FC	0	1.6E-03	5.8E-03	3.7E-03	1.4E-02	2.1E-03	1.0E-02
SIVsmE543-3	1.1	2.4E-03	>100	2.7E-03	>100	2.6E-03	80
SIVsmH805	7.5	16	>100	5.0	>100	5.2E-01	>100
SIVsmH807	6.9	>100	>100	9.1	>100	2.8	>100
SIVmac239	16.4	>100	>100	>100	>100	19	51
HIV-2_{GH123}	29.3	>100	>100	>100	>100	>100	>100
HIV-1_{NL432}	59.7	>100	>100	>100	>100	>100	>100

< 1.0E-02 | 1.0E-02 - 1.0E+00 | 1 - 100 | > 100 μg/ml

FIG 1 Potent and broad neutralization by monoclonal antibody B404 from a SIVsmH635FC-infected macaque. (A) The neutralizing potencies of IgG, Fab, and scFv of B404 are shown by inhibition kinetics against SIVsmE660FL14, SIVsmH805-24w-3, and SIVmac239. (B) The neutralizing potencies of IgG, Fab and scFv of B404 are shown by IC_{50} and IC_{90} (μg/ml). Seven SIV strains, HIV-2_{GH123} and HIV-1_{NL432} were examined for their neutralizing sensitivities against B404 in TZM-bl cells. The IC_{50} and IC_{90} values are shown in dark gray ($<1.0 \times 10^{-2}$ μg/ml), medium gray (1.0×10^{-2} to 1.0×10^{0} μg/ml), light gray (1 to 100 μg/ml) and white (>100 μg/ml). Percent amino acid differences were calculated by pairwise comparison with SIVsmH635FC.

tivity against 7 SIV strains (Fig. 1). These SIV strains were classified into 2 lineages, lineage 1 (SIVsmE660, SIVsmH635FC, SIVsmE543-3, SIVsmH805, and SIVsmH807) and lineage 8 (SIVmac316 and SIVmac239), according to the phylogenetic analysis by Apetrei et al. (63), which identified nine divergent lineages in SIVsm/mac corresponding to HIV-1 subtypes. Sensitivity to neutralization was known to be high in SIVmac316, SIVsmE660, and SIVsmH635FC (25, 38). Infection with these neutralization-sensitive SIV strains was almost completely blocked by low concentrations of all forms of B404. Although the potency to inhibit infection was similar among IgG, Fab, and scFv, B404 IgG was slightly more effective against these SIV strains, as shown by the neutralizing kinetics of SIVsmE660 (Fig. 1A). Neutralization of SIVsmE543-3, SIVsmH805, and SIVsmH807 reached a plateau at 10 to 100 ng/ml IgG B404 and Fab B404, as represented by neutralization kinetics against SIVsmH805 (Fig. 1A). These viruses were moderately sensitive to B404-mediated neutralization, although the IC_{50}s were variable among these SIV strains (Fig. 1B). Interestingly, B404 scFv was more effective at high concentrations than B404 IgG and B404 Fab in neutralization of these moderately neutralization-sensitive viruses and SIVmac239, which is a highly neutralization-resistant strain (Fig. 1). Infection with SIVmac239 was unaffected by the presence of any form of B404 at a concentration of less than 1 μg/ml but was inhibited more than 90% by 100 μg/ml B404 scFv. Neutralization of 7 of 7 SIV strains, including genetically diverse, neutralization-resistant SIVmac239, by B404 scFv indicates that B404 is a potent and broad NAb against SIVsm/mac strains.

Isolation of Env-specific Fab clones from SIVsmH635FC-infected macaques. To analyze the induction of B404-like antibodies in SIV-infected macaques, Env-specific Fab clones were isolated from 4 SIVsmH635FC-infected macaques: H723, H704, H709, and H714 (26, 39). Env-specific Fab clones from H723 were isolated from the previously constructed phage library (25) through panning against Env, which was conjugated by coating plate wells with the anti-Env Fab clones B404 (anti-gp120 conformational), B408 (anti-gp41 cluster I), and H301 (anti-gp120 V1). Together with anti-Env Fab clones from the previous study, 98 anti-Env Fab clones, including 33 NAbs (33.7%), were obtained from H723. From 3 other SIVsmH635FC-infected macaques, κ and λ light-chain phage libraries were separately constructed, and 2 panning series were performed using B404 and H301 to conjugate Env. After 4 series of panning in each macaque, we obtained 155, 102, and 53 independent Fab clones from H704, H709, and

TABLE 1 Preferential gene usage and competition with B404 of NAbs

Inoculated virus	Animal	Frequency (%) of NAbs[a]	No. of NAbs	% of NAbs with:		Avg CDRH3 length[b]	Competition (%) with B404[c]
				VH3 genes	λ light chains		
SIVsmH635FC	H723	33.7	33	81.8	93.9	20.0	81.8
	H704	30.3	47	95.7	97.9	18.7	100
	H709	7.8	8	75.0	100	17.8	100
	H714	52.8	28	96.4	92.9	18.7	100
SIV mix[d]	H711	17.2	15	26.7	40.0	15.2	86.7
	H725	2.2	1	0.0	100	12	100

[a] Frequencies of Fab clones with the VH3 gene and λ light chain are shown as percentages of NAbs.
[b] Average number of amino acids in CDRH3.
[c] Competition ELISA with 2 μg/ml B404 IgG was performed. The frequency of Fabs showing more than 50% inhibition is shown as a percentage of NAbs.
[d] H711 was inoculated with a mixture of SIVsmE543-3 and SIVsmH635FC. H725 was inoculated with plasma samples from 2 SIVsmH445-infected macaques, H631 and H635.

H714, respectively. Neutralizing activities were observed in 47 clones (30.3%) from H704, 9 clones (8.8%) from H709, and 28 clones (52.8%) from H714 (Table 1). Phylogenetic analysis of VH genes revealed that 105 NAbs formed a major NAb cluster with B404 (Fig. 2). The remaining NAbs were separated into 3 minor clusters containing 3 or 4 NAbs. Fab clones in the major group, designated the B404 group, were isolated from all 4 macaques analyzed.

Although Fab clones in the B404 group were genetically similar to one another, several small clusters were observed in the B404 group, suggesting multiple B cell origins generated by VDJ recombination in these B404-like NAbs. Sequence analysis using the International Immunogenetics Database (50) indicated that the VH genes of Fab clones in the B404 group were close to human pseudogene IGHV3-h (approximately 90% identity), but no functional VH gene showed >90% identity. Analysis using the genome database of the rhesus macaque (51) revealed a significant relationship (>95% identity) between Fab clones in the B404 group and the rhesus macaque VH3 gene in the chromosome 7 scaffold (GenBank accession number NW_001122023). These results suggest that a major group of NAbs in SIVsmH635FC-infected macaques preferentially use the same rhesus VH3 germ line that lacks a human counterpart.

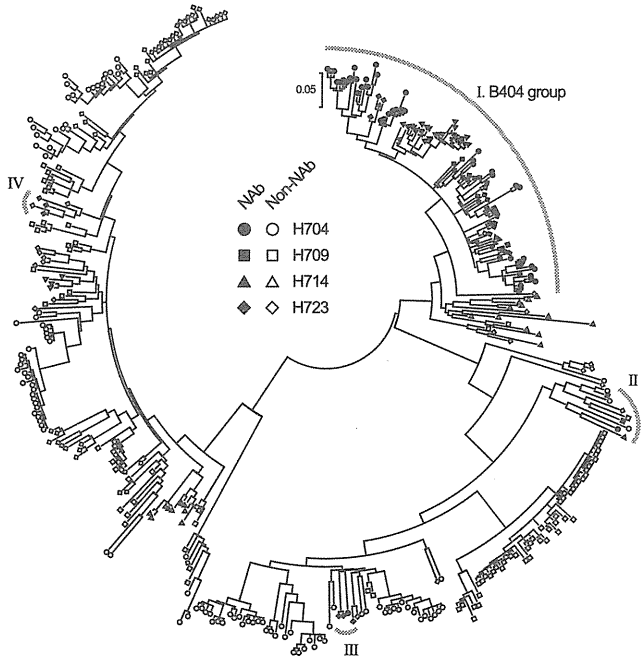

FIG 2 B404-like NAbs formed a major group in anti-Env antibodies from 4 SIVsmH635FC-infected rhesus macaques. NAbs were separated into 4 groups in the phylogenetic tree, which was generated using MEGA5 (70) from heavy-chain genes of 98, 155, 102, and 53 Fab clones from H704, H709, H714, and H723, respectively.

Bias in gene usage of NAbs from SIVsmH635FC-infected macaques. The genetic features of anti-Env Fab clones are summarized in Fig. 3 and Table 1. As mentioned above, a major population of NAbs from SIVsmH635FC-infected macaques used the same VH3 gene as B404, resulting in a high rate of NAbs using the VH3 gene (Fig. 3A and Table 1). A high occupancy of λ light chains was also characteristic of NAbs from SIVsmH635FC-infected macaques (Fig. 3B and Table 1). Moreover, a long complementarity-determining region 3 loop of the heavy chain (CDRH3) was characteristic of the NAbs (Fig. 3C and Table 1). CDRH3 of most NAbs had 19 or more amino acids, although the length of CDRH3 was usually less than 18 amino acids in nonneutralizing Fab clones. These results clearly showed that B404-like NAbs with the VH3 gene-encoded heavy chain with a long CDR3 and λ light chain are the main NAb population in SIVsmH635FC-infected macaques. In contrast, Fab clones from macaques H711 and H725 lacked these remarkable features of B404-like NAbs (Fig. 3, bottom; Table 1). These 2 macaques were inoculated with a mixture of SIVs (SIV mix). H711 was infected with a combination of SIVsmE543-3 and SIVsmH635FC. H725 was infected with plasma samples from 2 SIVsmH445-infected macaques, H631 and H635, which SIVsmH635FC was isolated from. Although anti-Env Fab clones were similarly isolated from these macaques, the frequency of NAbs from H711 (17.2%) and H725 (2.2%) was lower than that from SIVsmH635FC-infected macaques (8.8 to 52%). NAbs from H711 and H725 preferentially used VH1 gene-encoded heavy chains with a short CDRH3 and κ light chains, but NAbs from these macaques showed a genetic variation, similarly to those in HIV-1-infected patients (64). These results suggested that B404-like NAbs are induced exclusively in SIVsmH635FC-infected macaques.

Potent neutralizing activity and the same specificity of NAbs in the B404 group. To analyze the epitopes recognized by these NAbs, we first separated Fabs with neutralizing activity into 2 groups according to the results of competition ELISA with B404 IgG. All the NAbs in the B404 group and group II (Fig. 2) com-

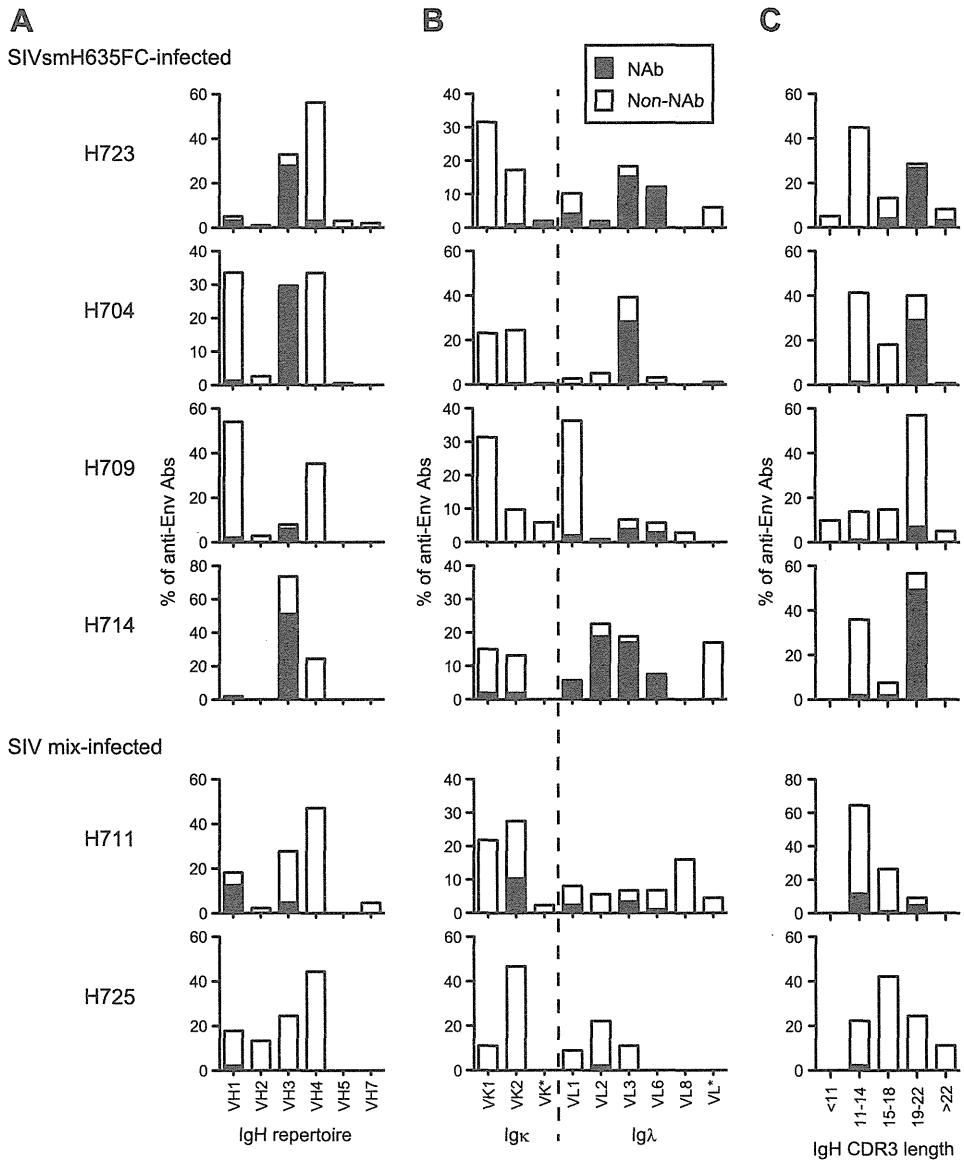

FIG 3 Bias in the Ig gene usage and CDR3 length of neutralizing Fab clones from SIVsmH635FC-infected macaques. The proportions of IgH (A) and Igκ and Igλ (B) repertoires and heavy-chain CDR3 length (C) are shown as percentages of NAbs and non-NAbs. In addition to Fabs isolated from 4 SIVsmH635FC-infected macaques, 87 Fab clones from H711, which was infected with a combination of SIVsmE543-3 and SIVsmH635FC, and 45 Fab clones from H725, which was infected with plasma samples from 2 SIVsmH445-infected macaques, H631 and H635, were similarly analyzed. Usage of Ig genes was analyzed using V-QUEST in the International Immunogenetics Database (44).

peted with B404 IgG (Fig. 4A), suggesting that epitopes for these NAbs overlap or are close to that for B404. Despite the differences in gene usage, competition with B404 IgG was also observed in most NAbs from macaques infected with SIV mix (Table 1). NAbs belonging to groups III and IV, with the exception of 1 Fab in group III, did not compete with B404 IgG (Fig. 4A). The binding ability of these Fabs was even enhanced by the addition of B404. Competition of the Fabs in groups III and IV with biotinylated K8 in group III suggested that the Fabs in group III and IV share the same epitope (data not shown). The neutralizing activity of these Fabs was examined against the genetically divergent SIVmac316 and the neutralization-resistant SIVsmE543-3 (Fig. 4B). All of the Fabs tested showed at least 50% inhibition against both viruses, and the B404 group included Fabs with potent neutralizing activity that showed efficient inhibition at low concentrations. Accordingly, the IC_{50}s of the 4 Fabs in the B404 group ranged from 0.8 to 316 ng/ml (average IC_{50}, 79 ng/ml) against SIVmac316, indicating the presence of NAbs comparable to B404 (IC_{50} against SIVmac316, 0.6 ng/ml) (Fig. 1). In contrast, IC_{50} against SIVmac316 ranged between 32 and 908 ng/ml (average IC_{50}, 243 ng/ml) in groups III and IV. This result suggests that B404-like NAbs are the main NAb population in terms of number and neutralizing potency.

Epitope mapping of NAb B404. To define the region of the Env targeted by B404, we examined reactivity against mutants of SIVsmE543-3 Env. Because the V3 loop has been shown to be important for B404 binding (25), mutants with deletions in the V1, V2, V3, and V4 loops (ΔV1, ΔV2, ΔV3, and ΔV4) and a mu-